

Numerical simulation of the syn- to post-depositional history of a prograding carbonate platform: the Rosengarten, Middle Triassic, Dolomites, Italy

AXEL EMMERICH*[†], ROBERT TSCHERNY*[§], THILO BECHSTÄDT*, CARSTEN BÜKER*[¶], ULLRICH A. GLASMACHER*, RALF LITTKE[‡] and RAINER ZÜHLKE*

**Geologisch-Paläontologisches Institut, Universität Heidelberg, Im Neuenheimer Feld 234, 69120 Heidelberg, Germany (E-mail: axel.emmerich@sap.com)*

[†]*RWE Dea AG, Überseering 40, 22297 Hamburg, Germany*

[‡]*Lehrstuhl für Geologie, Geochemie und Lagerstätten des Erdöls und der Kohle, RWTH Aachen, Lochnerstraße 4–20, 52056 Aachen, Germany*

[§]*IES GmbH, Ritterstraße 23, 52072 Aachen, Germany*

[¶]*Shell International E&P Inc., 200 North Dairy Ashford Street, Houston, TX 77079, USA*

ABSTRACT

A combination of thermal history, numerical basin-reverse and sequence-stratigraphic forward modelling is applied to the Mesozoic outcrop analogue of the Rosengarten carbonate platform area in the Dolomites of northern Italy. This integrated multidisciplinary approach of numerical simulation quantifies the thermal, subsidence, geometrical and subsequent facies evolution of the area. Calibration data during modelling were vitrinite reflectance (VR) and apatite fission-track (FT) analyses as well as detailed outcrop studies. Vitrinite reflectance values in strata underlying the carbonate platform vary between 0.5 and 0.8% VR_r; apatites from these formations reveal cooling ages of around 165.6 Ma and track lengths of approximately 9.8 µm. This low thermal maturity combined with the FT data in apatites indicates a relatively cool (<110°C), protracted (between 250 and 30 Ma) and shallow burial (thickness of eroded strata overlying present-day topography is <1100 m), as well as a fast exhumation from the Middle Miocene onward. Maximum temperatures are reached during the Middle/Late Triassic, when the basal heat flow was elevated owing to regional volcanic and hydrothermal activity. Local anomalies in vitrinite reflectance of up to 1.1% VR_r in the immediate surroundings of the Predazzo/Monzoni volcanic centre show that its thermal influence decreased rapidly with increasing distance. The geometrical evolution of the Middle Triassic (Anisian/Ladinian) Rosengarten platform is twofold: the first stage reveals aggradation, the second progradation of the platform margin. Basin-reverse modelling results indicate that these two intervals originate from a temporal change in tectonic subsidence. Spatial variations in flexural and tectonic subsidence along the 6 km transect are insignificant due to the rigidity of the basement (up to 2500 m of Late Permian ignimbrites). During the first stage of platform evolution, high pulse-like total subsidence rates of up to 820 m Myr⁻¹ led to aggradation, whereas the subsequent drop to 100 m Myr⁻¹ initiated platform progradation. The short-spanned subsidence peak was linked to block movements in a strike-slip tectonic setting (Cima Bocche Anticline-Stava Line approximately 10 km southeast of the study area). Stratigraphic forward modelling quantifies the sediment volumes involved in the geometrical evolution of the platform. In order to replicate platform architecture, constant carbonate accumulation rates between 900 and 1000 m Myr⁻¹ – increasing from periplatform environments to the slope – have to be assumed throughout the existence (approximately 5.8 Myr) of the Rosengarten. As the carbonate factory successfully keeps up with the modelled accommodation rates, it must have completely recovered from the Permian–Triassic biotic crisis during the onset of platform growth in latest Anisian times despite the low biotic diversity of the platform succession seen elsewhere in the Dolomites. Our forward modelling confirms that the main carbonate factory was situated on the slope at water depths from shallow subtidal to 300 m ('slope-shedding') and that it therefore switched on during all possible stages of accommodation change.

Keywords Basin analysis, numerical simulation, subsidence, thermal maturity, thermochronology, carbonate platform, aggradation, progradation, sedimentation rates, Triassic, Southern Alps, Dolomites.

INTRODUCTION

The Dolomites of northern Italy (Fig. 1) have long been a study area for carbonate platforms and their reef communities. Since Mojsisovics termed the word ‘Überguss-Schichtung’ back in 1879 (i.e., clinostratification), many authors have worked on platform-to-basin transitions of carbonate build-ups in the Dolomites (Hummel, 1928, 1932; Pia, 1937; Leonardi, 1962, 1967; Bosellini, 1984, 1988). In particular, the Rosengarten has served as a reference model for progradational geometries (Bosellini & Stefani, 1991; Bosellini *et al.*, 1996). However, assessing the evolution of carbonate platforms and their clinoforms has been mainly of a qualitative nature. Quantitative approaches of subsidence and carbonate accumulation of Middle Triassic platforms in the Dolomites have so far been scarce (Schlager, 1981; Doglioni & Goldhammer, 1988; Schlager *et al.*, 1991; Maurer, 1999, 2000; Keim & Schlager, 2001) and lack unbiased numerical modelling techniques. The age of these platforms is usually constrained by coeval basinal sediments containing abundant biostratigraphic information (Buchenstein Fm; Brack & Rieber, 1993, 1994). Recently, age-diagnostic airborne tuff layers in basinal and lagoonal strata were used to synchronize bio-, cyclo- and chronostratigraphy (basinal Buchenstein Fm at Seceda/Geisler Group, western Dolomites: Mundil *et al.*, 1996; lagoonal Schlern Dolomite Fm 1 at Latemar, western Dolomites: Mundil *et al.*, 2003; for locations see Fig. 2) providing a high-resolution database for numerical simulation. The particular feature of the Rosengarten platform is that some of these dated

tuff layers can be physically correlated to coeval slope deposits (Maurer, 1999, 2000).

The aim of this paper is the quantification of the development of the Rosengarten platform and the assessment of its primary controlling factors during platform growth. This is realized by an integrated approach of basin-reverse and stratigraphic-forward modelling combined with thermal basin modelling. Datasets for all modelling procedures are derived from existing studies and from new detailed analyses on allo-/sequence stratigraphy and facies architecture, thermal maturity and apatite fission tracks in strata underlying the platform body.

BASIN AND CARBONATE-PLATFORM DEVELOPMENT

The southwestern Dolomites (for location within the Alps, Fig. 1) are located on the Adriatic Plate between former Laurussia and Gondwana (Dercourt *et al.*, 2000). Throughout the Triassic, this area represents the eastern margin of a highly differentiated passive continental margin with mixed siliciclastic-carbonate sedimentation (Blendinger, 1985; Doglioni, 1987). First, carbonate ramps (early Anisian/Aegean) and small reef mounds (early in the late Anisian/Pelsonian) developed in the Dolomites (Fois & Gaetani, 1984; Senowbari-Daryan *et al.*, 1993) after the carbonate factory had eventually recovered from the severe faunal crisis at the close of the Permian. From the late Anisian into the late Ladinian, a considerable submarine relief with local subaerial highs prevailed in the western Dolomites. Middle Anisian transpressive-transtensive tectonics dismembered the continental shelf and created strong regional differences in facies (the so-called ‘Facies Heteropie’ *sensu* Bechstädt & Brandner, 1970; see also Zühlke, 2000). Deep marine, stagnant basins with fine-grained chert- and organic-matter-rich sediments (Anisian: Moena Fm and Anisian/Ladinian: Buchenstein Fm; Figs 2 and 3) existed alongside shallow marine subtidal carbonate ramps and platforms (Anisian: Contrin Fm and Anisian/Ladinian: Schlern Dolomite Fm 1; Figs 2 and 3). Structural highs of the dismembered carbonate ramp (Contrin Fm) represent the nuclei of the Schlern Dolomite Fm 1 platforms in the Late Anisian (Masetti & Neri, 1980; Gaetani *et al.*, 1981; Bosellini, 1989). Evolution of the Ladinian carbonate platforms such as the Rosengarten/Schlern, Monte Agnello and

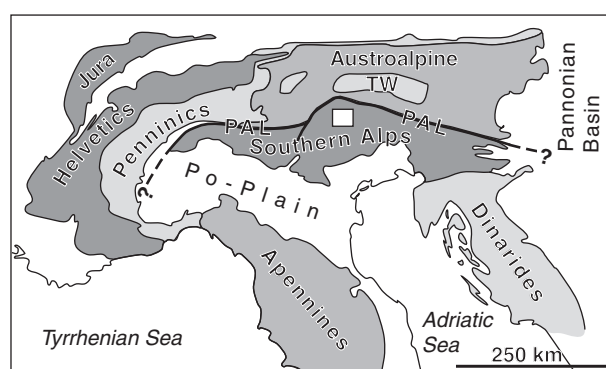


Fig. 1. Schematic tectonic map of the Alps. The white rectangle marks the location of the study area. Abbreviations: TW, Tauern window; PAL, Periadriatic lineament.

Fig. 2. Schematic palaeogeographical map of the western Dolomites during the Middle Triassic (late Anisian to early Ladinian) highlighting the distribution of platforms and basins. Legend of lithostratigraphic units in the upper-left corner, influx of Zoppé turbidite sands marked by large arrows. The volcanic centre of Predazzo–Monzoni in the immediate surroundings of the Rosengarten–Catinaccio platform is sketched with radial lines.

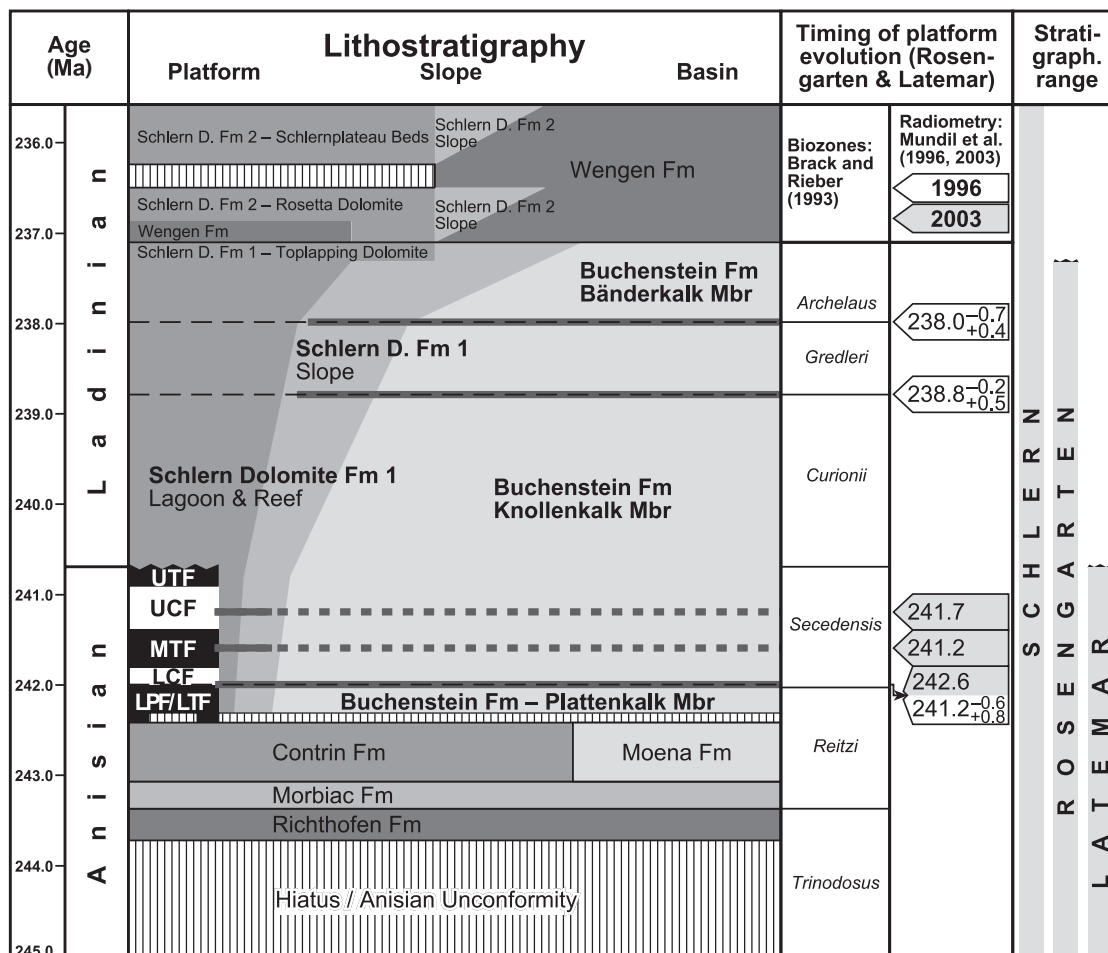
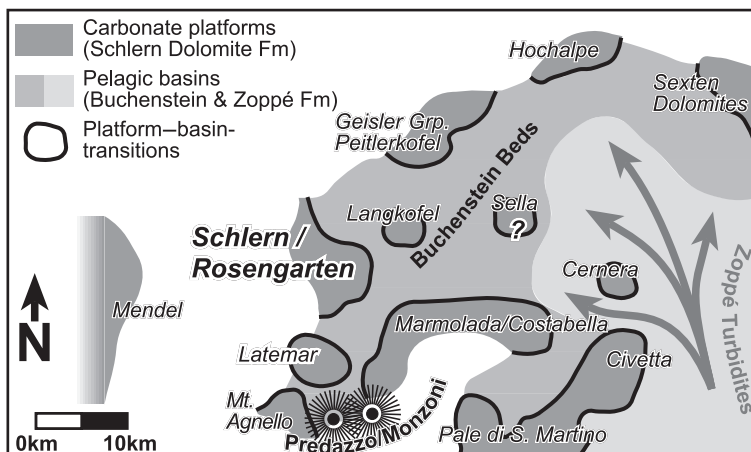


Fig. 3. Detailed Anisian–Ladinian lithostratigraphic succession of the study area (Schlern–Rosengarten and Latemar). The stratigraphic range of the carbonate platforms is illustrated on the right. Chronostratigraphy according to Lehrmann *et al.* (2002) and Mundil *et al.* (1996, 2003). Biozones and position of Anisian–Ladinian boundary according to Brack & Rieber (1993, 1994). Correlation of age-dagnostic tuff layers from basin to slope according to Maurer (1999, 2000). Hollow arrows in the radiometry column indicate ages from tuff layers in the basal Buchenstein Fm at Seceda (Geisler Group, western Dolomites; see Fig. 2; Mundil *et al.*, 1996) whereas light grey indicates ages from tuff layers in the lagoonal Schlern Fm at Latemar (western Dolomites; see Fig. 2; Mundil *et al.*, 2003).

possibly also the Latemar was terminated by the extrusion of the Longobardian Wengen Group volcanics (Mojsisovics, 1879; Viel, 1979a, 1979b; De Zanche *et al.*, 1995; Fig. 3). The volcanic centre at Predazzo/Monzoni was nourished by a source linked to a deep-reaching fracture zone (Cima Bocche Anticline/Stava Line; Fig. 4; Blendinger, 1985). Tectonics also played a crucial role in platform development in the southwestern Dolomites as regional subsidence and accommodation development were controlled by downward movements along faults and upward movements through magmatic updoming (Doglioni, 1983, 1984, 1987).

Owing to its excellent, laterally continuous seismic and sub-seismic scale outcrop (Fig. 5a and b), the Rosengarten part of the Rosengarten/Schlern platform is ideally suited for a study on the geometric development of a carbonate platform and its accumulation rates. The platform top of the Rosengarten passes laterally into a platform slope interfingering with basinal sediments. The maximum north to south progradation of the Rosengarten slope was approximately 6 km. Lagoon, reef and slope facies of the build-up are all part of the Schlern Dolomite Formation 1, whereas coeval basinal sediments belong to the Buchenstein Formation. Bio- and chronostratigraphic data (Brack & Rieber, 1993, 1994; Mundil *et al.*, 1996, 2003; Maurer, 1999, 2000; Fig. 4) indicate the onset of platform growth in the upper *Reitzi*-biozone (Anisian; Middle Triassic stages after Brack & Rieber, 1993, 1994). According to Maurer (1999, 2000), the slope of the Rosengarten records five ammonite biozones (Fig. 5b). During the first two – *Reitzi* and *Secedensis* – biozones of platform existence, aggradation occurred. This first stage of platform evolution was followed by a second stage of progradational clinofolds. The preserved record of carbonate sedimentation lasted at least until the basal *Archelaus*-zone (middle/late Ladinian; Maurer, 1999, 2000; Fig. 5b). The maximum thickness of the Rosengarten – and therefore also its growth mode – can be inferred only by projecting stratigraphical information from the Schlern platform (Bosellini & Stefani, 1991; Fig. 6). At Schlern, 850 m of cyclically arranged platform carbonates are partially covered by Wengen Group volcanics (Fig. 4) preserving the maximum thickness of the Schlern Dolomite Fm 1 (Fig. 3). Using all available biostratigraphic data, Maurer (1999, 2000) estimated compacted carbonate accumulation rates for the first aggradational phase of 200 m Myr^{-1} increasing during the second progradational phase.

As the oldest rocks in the study area that have been preserved belong to the uppermost Ladinian, the geological evolution from Late Triassic times onward can be derived only by studying younger successions in other parts of the Dolomites (e.g. Sella platform, Fig. 2) and the Southern Alps (e.g. Trento platform). Late Triassic volcanoclastics and carbonates (Wengen Group; Mastandrea *et al.*, 1997) filled the basins. An extensive carbonate platform developed with the onset of a period of tectonic quiescence. The so-called Trento platform comprises the entire central segment of the Southern Alps on the Adriatic Plate (Dolomia Principale Fm and Calcari Grigi Fm; Leonardi, 1967; Bosellini & Broglio Loriga, 1971; Bosellini & Hardie, 1985; Trevisani, 1991; Boomer *et al.*, 2001). From Middle Jurassic times onward, the Trento platform started to subside and eventually drowned. A phase of deep marine sedimentation began (Ammonitico Rosso Fm; Winterer & Bosellini, 1981; Martire, 1996; Winterer, 1998) and lasted until Late Cretaceous times (Marne del Puez Fm; Claps *et al.*, 1991; Antruilles Fm; Stock, 1996). Water depths decreased when the tectonic regime switched from extensional to compressional and the collision of the Adriatic plate with Europe began with Late Cretaceous subduction of oceanic crust (Hsü, 1971; Smith, 1971; Trümpy, 1982; Laubscher & Bernoulli, 1982; 'eoalpine' *sensu* Doglioni & Bosellini, 1987; Hsü, 1989). Towards the east, the Southern Alps were strongly involved in the Dinaric orogeny during the Late Eocene, but the compression front is thought to have extended even into the Dolomites (Doglioni & Bosellini, 1987). This interval of convergence was shortly interrupted by an Oligocene extensional phase recorded along the Periadriatic Line by plutonic intrusions (e.g. Adamello pluton) and dykes as well as by effusive basalts at the southwest termination of the Trento Plateau (Zattin *et al.*, 2006). Upper Oligocene shallow-marine conglomerates (Monte Parei Fm) record uplifted source areas during ongoing or renewed continent collision in the eastern Dolomites (Cros, 1966; Mair *et al.*, 1996). Although steady state or episodic exhumation of parts of the Alps remains debated (Bernet *et al.*, 2001; Carrapa *et al.*, 2003; Kuhlemann *et al.*, 2006), there seems to be increasing consensus on the timing of exhumation. At least three stages of exhumation are observed: rapid exhumation before approximately 35 Ma, slower exhumation until ~15 Ma and very rapid exhumation to present-day positions from then onward

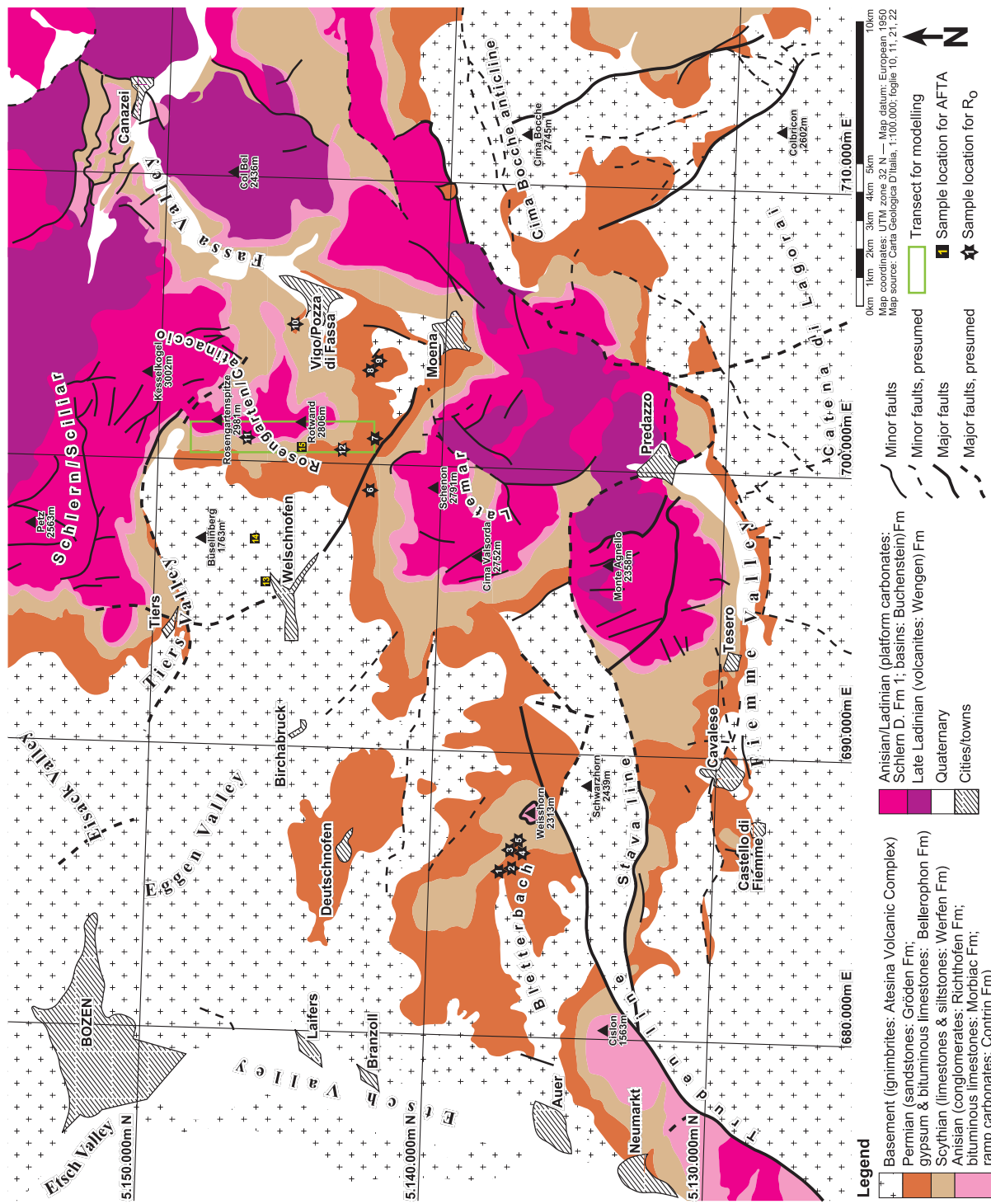


Fig. 4. Simplified geological map of the study area and its surroundings. Note the presence of the Cima Bocche Anticline/Stava Line (major faults) and the late Ladinian Wengen Group volcanics in the eastern and northeastern part of the area. Legend of the geological map in the lower part. Sample locations for vitrinite-reflectance analyses are marked by stars, those for apatite fission-track analyses by squares.

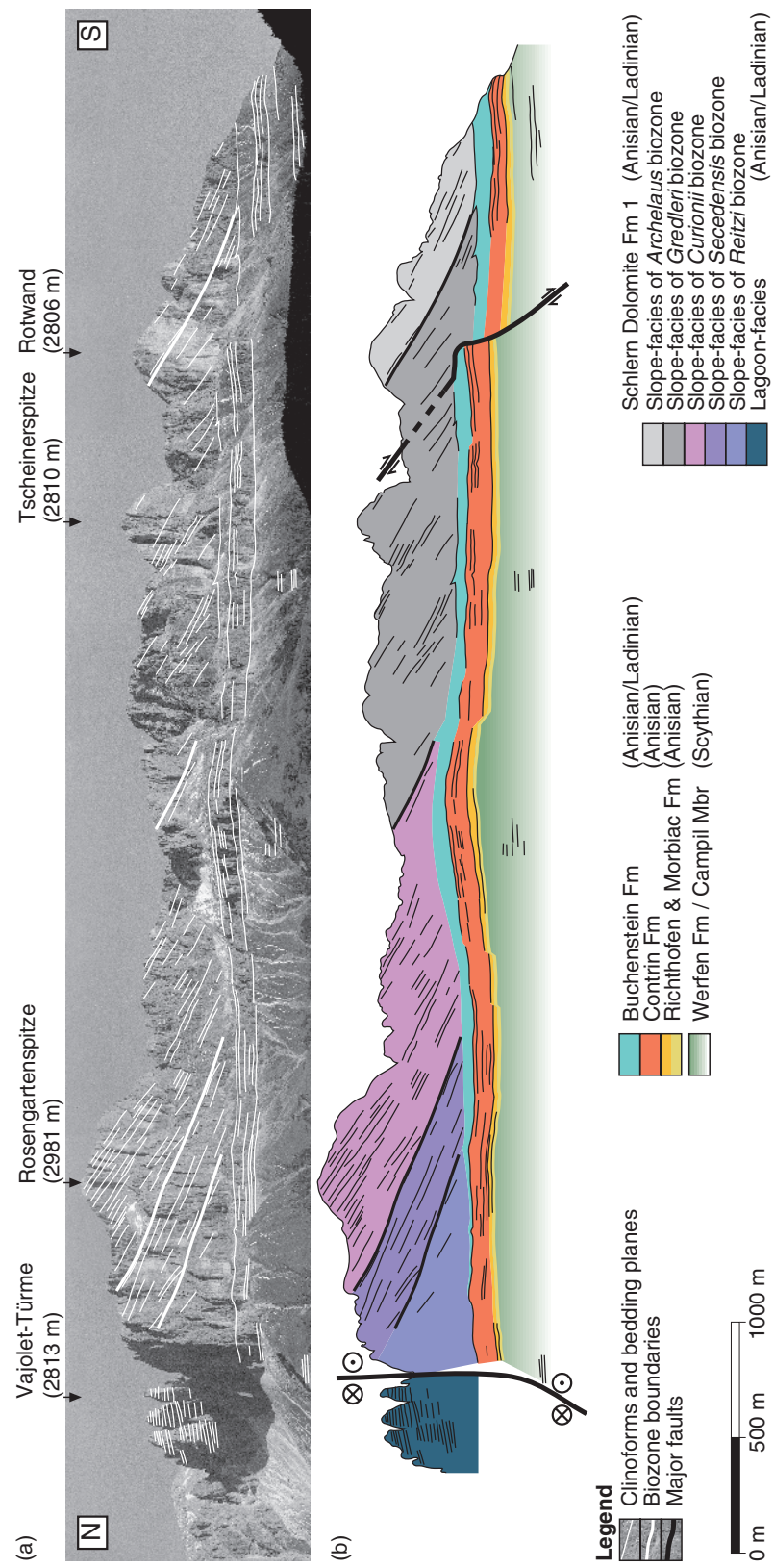


Fig. 5. Sedimentological interpretation of the Rosengarten platform. (a) The Rosengarten platform viewed from the west with an interpretation of stratal lines and clinoforms. The location of the transect is marked in Fig. 4. Legend underneath Fig. 5b. (b) Formations underneath the Rosengarten platform and correlation of carbonate slope deposits with biozones of the basal Buchenstein Fm (according to Maurer, 1999, 2000). The transect is tectonically undisturbed, major faults are present at the platform interior only ('Vajolet-Türme'/'Torri del Vajolet').

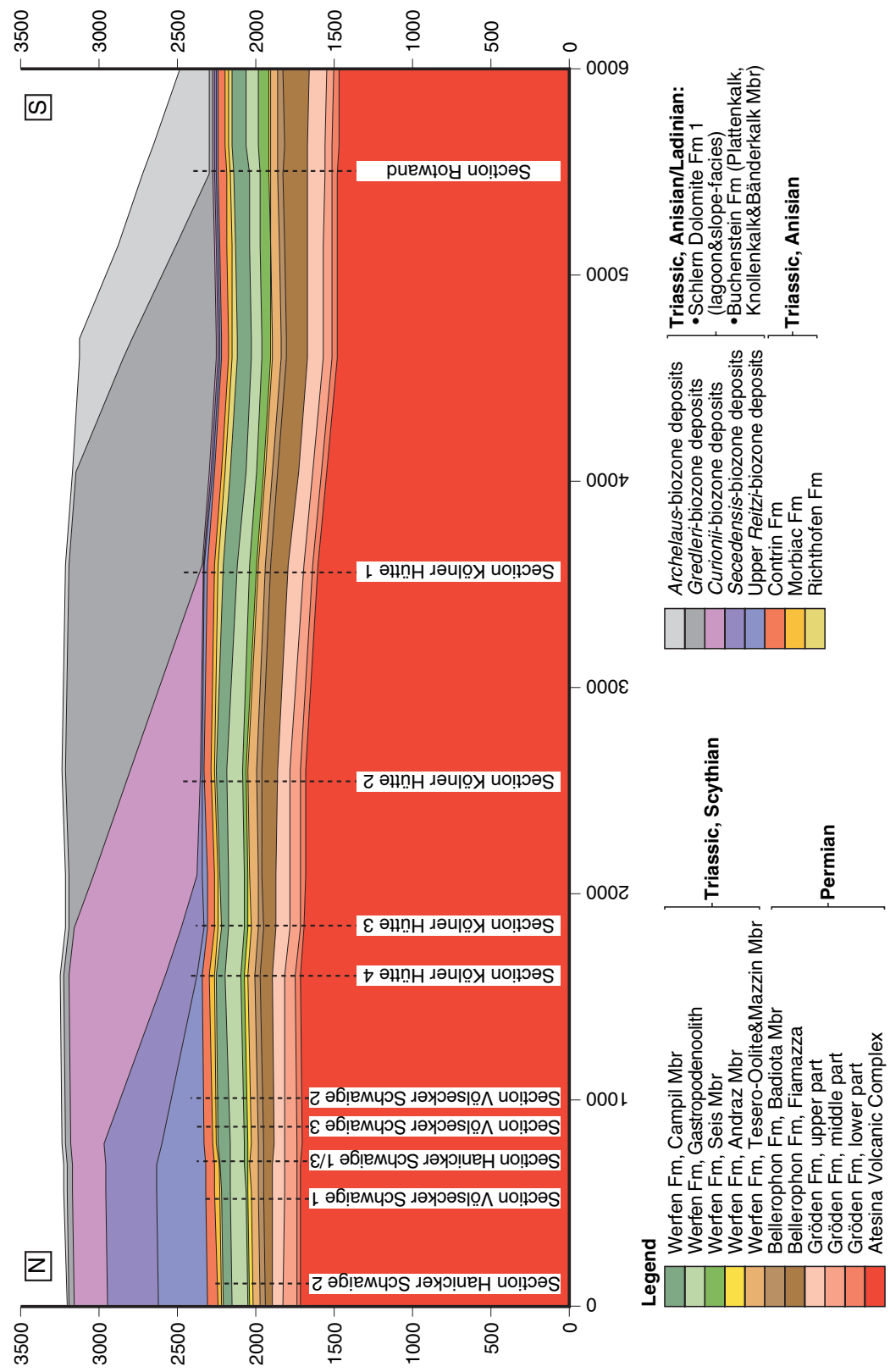


Fig. 6. The Rosengarten transect with restored geometries above present-day topography (after Bosellini & Stefani, 1991; Maurer, 1999, 2000) with an overlay of formations, and intervals of platform growth (colour code in the lower part). The sedimentological sections logged through the underlying strata of the Schlern Dolomite Fm I during the course of this study are indicated. Vertically exaggerated; units of the x-axis are metres along the transect beginning at the platform interior; units of the y-axis are metres above mean present-day sea level.

(Carrapa *et al.*, 2003; Zattin *et al.*, 2003; Bertotti *et al.*, 2006).

METHODS AND DATABASE

Sedimentological analyses

Detailed sedimentological analyses (logging, facies mapping, lateral tracing of physical surfaces, thin sections) have been carried out on the underlying strata of the Rosengarten platform (Fig. 6). Ten sections/sedimentological logs cover the entire basin fill from basement (Atesina Volcanic Complex, AVC) to the basal Schlern Dolomite Fm 1. Additional data on the upper Anisian succession and the Buchenstein Fm were taken from the literature (Bosellini & Stefani, 1991; Maurer, 1999; Zühlke, 2000). These analyses are necessary to obtain datasets on thicknesses, lithologies and palaeowater depths. The latter is based on the integration of all sedimentological evidence from the outcrops (channels, ripples, exposure surfaces, bioturbation, etc.) combined with microfacies analyses of the 283 thin-sections.

Stratigraphy and timescale

Within the past years, there has been some controversy about the duration of Schlern Dolomite Fm 1, informally known as the 'Latemar controversy' (Brack *et al.*, 1997; Hardie & Hinnov, 1997). Several studies (Goldhammer & Harris, 1989; Hinnov & Goldhammer, 1991; Preto *et al.*, 2001) proposed a specific type of orbital forcing for the cyclically arranged lagoonal interior of the Schlern Dolomite Fm 1. Subsequent studies (Brack & Rieber, 1993; Brack *et al.*, 1996; Mundil *et al.*, 1996) questioned this Milankovitch model because of its incompatibility with bio- and chronostratigraphic data. Radiometric age dating on detrital zircons in airborne tuff layers intercalated within the lagoonal sediments of the Latemar helped to solve the controversy (Mundil *et al.*, 2003). Subsequent time-series analyses and numerical simulation based upon *in situ* bio- and chronostratigraphic data indicate a much higher frequency of the cycles and thus a much shorter duration of the entire cyclic succession (Zühlke *et al.*, 2003; Zühlke, 2004; Emmerich *et al.*, 2005a). This study follows the stratigraphic concept laid down in Emmerich *et al.* (2005a).

Upper Triassic formations were evaluated and thicknesses projected from the western and central

Dolomites (Schlern, Sella and Gardenaccia platform), Jurassic strata from the Trento platform, and Cretaceous and Tertiary formations from the eastern Dolomites (Table 1). Lithology information was combined with published data on chronostratigraphy and palaeobathymetry. Initial Jurassic palaeowater depths were calculated with a subsidence curve for the Trento platform proposed by Winterer & Bosellini (1981) and Winterer (1998). If necessary, thickness of eroded stratigraphic units and palaeowater depth were adapted within a range of values provided by studies on the regional geology (Table 1) in order to fit the simulated time-temperature evolution.

The timescale applied during modelling (Table 1) was determined by subdividing known chronostratigraphic intervals by biostratigraphical information (for details on this method see Bosence *et al.*, 1994; Aurell *et al.*, 1998). This means that existing studies on the temporal evolution of the Upper Permian (basement: Barth & Mohr, 1994; Barth *et al.*, 1993, 1994; sedimentary cover: Massari & Neri, 1997), Lower Triassic (Broglio Loriga *et al.*, 1983) and Middle Triassic (Brack & Rieber, 1993; Brack *et al.*, 1996; Maurer, 2000; Zühlke, 2000; Zühlke *et al.*, 2003) in the study area were recalibrated to latest radiometric age measurements (Permian: Yugan *et al.*, 1997; Permian-Triassic boundary: Mundil *et al.*, 2001; Lower Triassic: Lehrmann *et al.*, 2002; Middle Triassic: Mundil *et al.*, 1996, 2003). The relative duration of the bio-, sequence- and lithostratigraphic timesteps of the existing studies was left unchanged. Younger chronostratigraphic ages were derived from the *Geological Time Scale 2004* (Gradstein *et al.*, 2004).

Vitrinite reflectance and apatite fission-tracks

Vitrinite reflectance (VR) is the most frequently used parameter in assessing regional thermal maturity and is furthermore widely used as a calibration parameter for numerical simulation of thermal basin development. Vitrinite reflectance data on seven sample locations were previously published (Buggisch, 1978; Schulz & Fuchs, 1991; Bielefeld, 1998; Table 2). One location was included where T_{\max} data were available that complemented the published dataset on thermal maturity (Zattin *et al.*, 2006; Table 2). In addition to this dataset, 11 samples from Upper Permian sandstones (Gröden Fm) to Middle Triassic basinal shaly limestones (Buchenstein Fm) were analysed in this study. Vitrinite reflectance was determined

Table 1. List of formations/timesteps (column 2) applied during modelling with ages at tops of formations/timesteps (column 3), thicknesses (column 4), indication of erosion (column 5) and lithologies (column 6). The last column (column 7) shows the main references for these formations with respect to the information shown in this table. The chronostratigraphic framework is derived from the following literature: Permian (Yugan *et al.*, 1997), Triassic (Lehrmann *et al.*, 2002; Mundil *et al.*, 1996, 2001, 2003), Jurassic, Cretaceous and Cenozoic/Tertiary (Gradstein *et al.*, 2004). Strata overlying present-day topography were projected from the western and central Dolomites (Middle and Upper Triassic; see also Fig. 4), the Trento platform (Jurassic) and eastern Dolomites (Cretaceous and Tertiary).

Era	Formation/timestep	Age (Ma)		Thickness (m)	Erosion	Lithology	Reference
		From	To				
TERTIARY	Monte Parei Fm	28.0	24.0	90	Yes	Conglomerate with interbedded sst	8,9
	Hiatus	80.0	28.0	-	Yes	-	8,9
	Antruilles Fm	98.9	80.0	70	Yes	lst with interbedded sst and clay	10
	Marne del Puezz Fm	127.0	98.9	60	Yes	Marl with interbedded fine-grained sst	11
JURASSIC	Hiatus	147.5	127.0	-	Yes	-	12,13
	Ammonitico Rosso Fm, upper part (RAS)	154.0	147.5	10	Yes	lst with interbedded silt	12,13,14
	Hiatus	155.5	154.0	-	Yes	-	12,13,14
	Ammonitico Rosso Fm, middle part (RAM)	157.0	155.5	5	Yes	lst with interbedded silt	12,13,14
	Hiatus	160.0	157.0	-	Yes	-	12,13,14
	Ammonitico Rosso Fm, lower part (RAL)	167.0	160.0	15	Yes	lst with interbedded silt	12,13,14
	Hiatus	169.0	167.0	-	Yes	-	12,13,14
	Calcare a Filamenti Fm	172.0	169.0	20	Yes	lst	15
	Hiatus	174.0	172.0	-	Yes	-	15
	San Vigilio Oolite Mbr	178.0	174.0	70	Yes	lst	15
	Calcare Grigi Fm, Grigno Mbr	183.6	178.0	90	Yes	lst	15
	Calcare Grigi Fm, Rotzo Mbr	190.0	183.6	85	Yes	lst	15,16
	Calcare Grigi Fm, Middle Mbr	194.5	190.0	35	Yes	lst	16,17
	Calcare Grigi Fm, Lower Mbr	200.0	194.5	40	Yes	lst	16,17
TRIASSIC	Dolomia Principale Fm, upper part	207.9	200.0	40	Yes	Dolomite	18,19
	Dolomia Principale Fm, middle part	215.8	207.9	175	Yes	Dolomite	18,19
	Dolomia Principale Fm, lower part	223.8	215.8	100	Yes	Dolomite	18,19
	Raibl Fm	229.9	223.8	40	Yes	Sandy lst	18,20,21,22
	Hiatus	232.0	229.9	-	Yes	-	18,20,21,22
	Wengen Fm, Schlern Dolomite Fm 2, Cassian Fm	237.1	232.0	100-730	Partially	Volcanics with lst boulders, dolomite, shale dolomite	21,22,23,24
	Archeilus biozone deposits (Schlern Dolomite Fm 1 & Buchenstein Fm)	238.0	237.1	20-400	Partially		22,25,26,27,28
	Gredleri biozone deposits (Schlern Dolomite Fm 1 & Buchenstein Fm)	238.8	238.0	18-800	Partially	Dolomite	22,25,26,27,28
	Curioni biozone deposits (Schlern Dolomite Fm 1 & Buchenstein Fm)	241.0	238.8	12-640	Partially	Dolomite	22,25,26,27,28

(Continued.)

Table 1. Continued.

1	2	3		4	5	6	7
		Age (Ma)					
Era	Formation/timestep	From	To	Thickness (m)	Erosion	Lithology	Reference
TRIASSIC (<i>Continued</i>)	<i>Secedensia</i> biozone deposits (Schlern Dolomite Fm 1 & Buchenstein Fm)	242.3	241.0	10–300	Partially	Dolomite	22,25,26,27,28
	<i>Reitzi</i> biozone deposits (Schlern Dolomite Fm 1 & Buchenstein Fm)	242.9	242.3	10–300	No	Dolomite	22,25,26,27,28
	Contrin Fm	243.5	242.9	40–55	No	Dolomite	22,29
	Morbiac Fm	243.8	243.5	25	No	Marl with interbedded lst	22,29
	Richthofen Fm	244.2	243.8	7–25	No	Conglomerate with interbedded coarse-grained sst	22,29
	Hiatus	247.5	244.2	–	No	–	22,29
	Werfen Fm, Cencenighe Mbr	248.1	247.5	80	Yes	lst with interbedded marl	30
	Werfen Fm, Val Badia Mbr	248.7	248.1	60–80	Partially	Marly lst	30
	Werfen Fm, Campil Mbr	250.0	248.7	45–90	Partially	Fine-grained sandstone with interbedded silt	22,30
	Werfen Fm, Gastropodenoolith Mbr	250.6	250.0	60–100	No	Intercalations of lst, marl and silt	22,30
	Werfen Fm, Seis Mbr	251.5	250.6	12–55	No	Intercalations of lst and marl	22,30
	Werfen Fm, Andraz Mbr	252.0	251.5	12–20	No	Sandy dolomite	22,30
	Werfen Fm, Tesero Oolite & Mazzin Mbr	253.0	252.0	40–50	No	Intercalations of lst, marl and silt	22,30
PERMIAN	Bellerophon Fm, Badiota Mbr	253.8	253.0	25–35	No	Intercalations of lst and marl	22,31,32,33,34
	Bellerophon Fm, Fiamazza Mbr	255.3	253.8	50–150	No	Gypsum with interbedded dolomitic marl	22,31,32,33,34
	Gröden Fm, upper part	256.6	255.3	65–105	No	Silt-rich medium- to fine-grained sst	22,32,33,34
	Gröden Fm, middle part	258.0	256.6	45–75	No	Silt-rich coarse-grained sst	22,32,33,34
	Gröden Fm, lower part	260.0	258.0	25–35	No	Litharenitic sst	22,32,33,34
	Hiatus	267.0	260.0	–	No	–	22,32,33,34
	Atesina Volcanic Complex	276.0	267.0	>2000	Partially	Rhyolitic ignimbrites, sometimes interbedded sediments	35,36,37,38

Key to column 7 (reference):

8: Cros 1966; 9: Mair *et al.* 1996; 10: Stock 1996; 11: Claps *et al.* 1991; 12: Winterer & Bosellini 1981; 13: Winterer 1998; 14: Martire 1996; 15: Trevisani 1991; 16: Bosellini & Broglio Loriga 1971; 17: Boomer *et al.* 2001; 18: Leonardi 1967; 19: Bosellini & Hardie 1985; 20: Doglioni & Goldhammer 1988; 21: Brandner 1991; 22: this study; 23: Schlegler *et al.* 1991; 24: Mastandrea *et al.* 1997; 25: Brack & Rieber 1993; 26: Brack & Rieber 1994; 27: Maurer 1999; 28: Maurer 2000; 29: Zühlke 2000; 30: Broglio Loriga *et al.* 1983; 31: Buggisch & Noé 1986; 32: Massari *et al.* 1988; 33: Massari *et al.* 1994; 34: Massari & Neri 1997; 35: D'Amico & Del Moro 1988; 36: Barth *et al.* 1993; 37: Barth *et al.* 1994; 38: Barth & Mohr 1994.

Fm., Formation; Mbr., Member; sst., sandstone; lst., limestone; RAS: rosso ammonitico superiore; RAM: rosso ammonitico mediore; RAI: rosso ammonitico inferiore.

Table 2. List of vitrinite reflectance, thermal maturity and apatite fission-track data. The numbers in the first column correspond to the locations in Fig. 4. The source of the data and their sample numbers are shown in columns 2 and 3. UTM coordinates (column 4) and elevations above present-day sea level (column 5) correspond to the system and map datum used in Fig. 4. The formations from which the samples were taken are listed in column 6. The lithology of the samples is shown in column 7. Columns 8–10 list data on thermal maturity. Palaeotemperature values in column 9 are calculated from the measured thermal maturity data (% VR_r values in column 8) after the equation of Barker & Pawlewicz (1986). The last columns (11, central age; 12, mean track length) refer to the apatite fission-track analysis carried out in Emmerich *et al.* (2005).

1	2	3	4	5	6	7	8	9	10	11	12
Loc.	Reference	Sample number	UTM coordinates x y	Elevation (m)	Formation member	Lithology*	VR _r (%)	Calculated T (°C)	T _{max} (°C)	Central age (Ma)	Mean track length (μm)
1	Buggisch 1978	Bb40	685800 5137100	1520	Gröden, middle part	Sandstone	0.73	110			
2	Bielefeld 1998	15e, 15eII	685800 5137100	1520	Gröden, middle part	Sandstone	0.60 ± 0.09	94 ± 11			
3	Bielefeld 1998	Butter2, But	686750 5136900	1650	Gröden, upper part	Sandstone	0.68 [†]	104			
4	Buggisch 1978	Bb, Bb10	686750 5136900	1650	Gröden, upper part	Sandstone	0.62 [†]	97			
5	Schulz & Fuchs 1991	–	686750 5136900	1650	Gröden, upper part	Sandstone	0.88	125			
6	Bielefeld 1998	20a, 20aII	698900 5142550	1710	Gröden, upper part	Sandstone	0.76 ± 0.10	113 ± 10			
7	Bielefeld 1998	N6a, N6b, N6bII	701000 5142350	1620	Gröden, upper part	Sandstone	0.67 ± 0.14	103 ± 15			
8	This study	groed 1	703493 5142526	1600	Gröden, upper part	Sandstone	0.9 ± 0.07 [‡]	127 ± 6			
9	This study	groed 2	703493 5142526	1600	Gröden, upper part	Sandstone	1.1 ± 0.14 [‡]	143 ± 10			
10	This study	belle	705014 5145331	1615	Bellerophon, Badiota	Limestone	0.52 ± 0.02	83 ± 3			
11	This study	070	700900 5148006	2330	Morbiac	Limestone	0.77 ± 0.02 [§]	114 ± 2	462		
12	Zattin <i>et al.</i> 2006	12	700500 5144460	1520	Moena	Limestone			429		
13	Emmerich <i>et al.</i> 2005b	AE14	695807 5145764	1275	Atesina Volcanic Complex	Ignimbrite, rhyolitic				84.2 ± 12.7 [¶]	10.6 ± 1.5
14	Emmerich <i>et al.</i> 2005b	AE18	697212 5146488	1450	Atesina Volcanic Complex	Ignimbrite, rhyolitic				165.6 ± 7.3	9.8 ± 1.6
15	Emmerich <i>et al.</i> 2005b	AE10	701149 5144079	2160	Werfen, Gastropoden-Oolith	Sandstone				74.7 ± 8.1 [¶]	10.8 ± 1.9

* Coarse to medium-grained sandstones, except sample AE10, which is fine-medium grained. The total organic carbon of limestone is <1%.

† Organic matter not *in situ* or altered.

‡ Proximity to a volcanic dyke, altered organic matter.

§ Number of measurements too low, no statistical significance.

¶ Number of grains too low, no statistical significance.

by microscopic analysis of percentages of light reflected from polished organic particles and calibrated against isotropic standards. The results are given as mean random reflectance (% VR_r , for details on methodology and measurement see Stach *et al.*, 1982; Taylor *et al.*, 1998). Only four of our samples – mostly Permian sandstones of the Gröden Fm – contained measurable ‘vitrinite-like’ organic matter (locations are shown in Fig. 4 and data are documented in Table 2). Several VR_r values had to be excluded as calibration parameters in thermal history modelling because of altered organic matter and/or statistically insignificant measurements (see also Table 2). As the time component is lacking in vitrinites, apatite fission-track (FT) thermochronology is commonly used to determine the magnitude and timing of cooling, exhumation and rock uplift from shallow crustal levels (Fitzgerald *et al.*, 1995; Tippett & Kamp, 1995). An extensive study on the surroundings of the Rosengarten has already been carried out by Emmerich *et al.* (2005a). Time–temperature paths from this study were used to calibrate the thermal history of the basin (Table 2).

Workflow of the integrated numerical modelling approach

The challenge during numerical simulation of present-day subaerially exposed areas is the determination of the amount and lithology of eroded overburden. Usually this is realized by extrapolating known successions to the study area but this dataset has to be verified iteratively during thermal modelling calibrated with data on thermal maturity and thermochronology. Hence, numerical simulation in this project started with modelling the burial and thermal history of the Rosengarten transect and the reconstruction of its overburden thickness with PetroModTM (IES GmbH, Aachen, Germany). Essential input parameters were lithology, sediment–water interface temperatures (SWI, Fig. 8a), palaeowater depths (PWD, Fig. 8b) and heat-flow development (Fig. 8c). Results on the eroded rock column were obtained by fitting calculated and measured vitrinite reflectance data (Fig. 9) as well as by forward modelling t – T paths, fission-track distributions and cooling ages in apatites (Fig. 10). The eroded thickness derived from numerical simulation was entered with all other necessary input parameters (Fig. 7) into the inverse modelling routine of PHILTM (Petrodynamics Inc., Houston, USA) in order to determine tectonic-, flexural- and

compaction-induced subsidence rates for forward simulation of sedimentation. The stratigraphic forward modelling module of PHILTM was used to calculate best-fit stratal patterns and sedimentation rates. At the end of this workflow, simulated minimum–maximum models were ultimately checked against the real-world/outcrop data. Calibration of the simulated sedimentation rates and stratal patterns was hereby performed by visual comparison with observed geometries along the Rosengarten transect and by measurement of stratal thicknesses.

Thermal modelling

Thermal modelling (in addition to petroleum systems or basin modelling) is now routinely used in petroleum exploration (Welte *et al.*, 1997; Makhous & Galushkin, 2004). Numerical simulation software usually incorporates geological, petrophysical, geophysical and geochemical data into integrated four-dimensional (4D) frameworks that allow testing of burial and basin-fill concepts. The geohistory of basins is subsequently recreated by these 4D simulations in three spatial dimensions through geological time. The accuracy of numerical simulations is limited by restricted knowledge of or uncertainty about the values of the input parameters used to constrain the basin history (Peters *et al.*, 2006).

The detailed analysis of the regional thermal maturity (coalification) pattern was combined with fission-track analyses in apatites in order to narrow down these uncertainties of thermal boundary conditions (heat-flow history). The timing and magnitude of intervals characterized by subaerial exposure and erosion were determined (i.e., burial history or geohistory of the basin). Input parameters for the numerical models were thicknesses of stratigraphic units, lithologies (Table 1), petrophysical parameters (e.g. thermal conductivities; see Bükler (1996) and Hertle & Littke (2000) for a more detailed description of the calculation of physical properties of stratified sediment bodies), temperature at the sediment–water interface (Fig. 8a), palaeowater depths (Fig. 8b) and heat flow at the base of the succession (Fig. 8c). Subsidence history and temperature field through time were subsequently calculated. Burial and heat-flow histories were continuously calibrated using measured vitrinite reflectance values (Fig. 9) and fission-track data derived from apatites (Fig. 10b). The model was

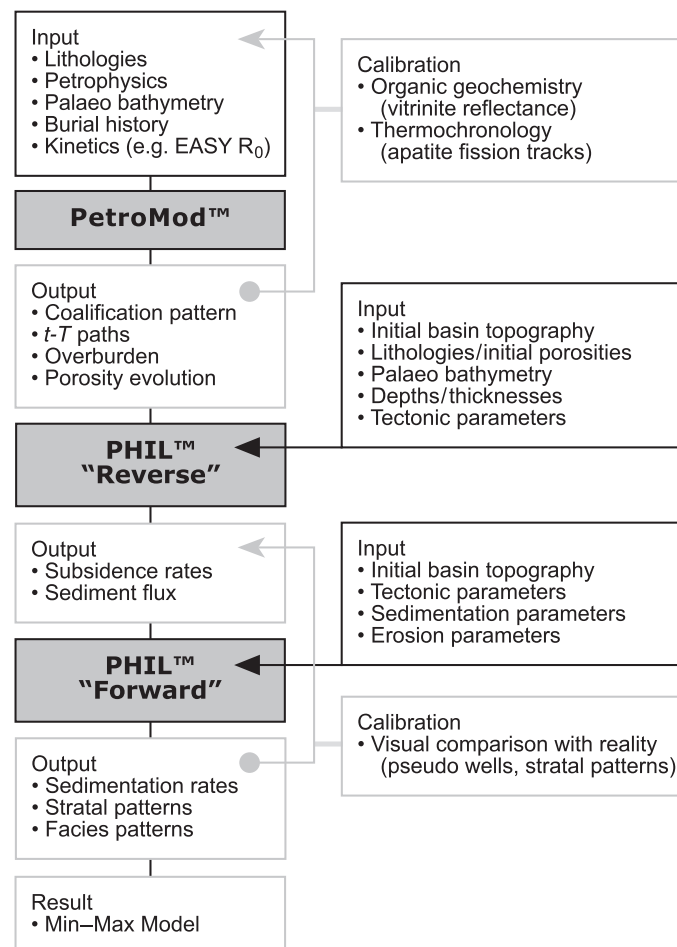


Fig. 7. Sketch illustrating the workflow during modelling; workflow starts at the top and ends at the bottom. Input data are arrows towards a simulator (PetroMod™ or PHIL™); output data used for calibration are lines away from simulators.

then fine-tuned by modifying all input parameters until a satisfactory fit between measured and calculated calibration data was achieved. Vitrinite reflectance was calculated using the EASY% R_0 -algorithm of Sweeney & Burnham (1990; Sachsenhofer & Littke, 1993; Littke *et al.*, 1994; Leischner, 1994; Sachsenhofer *et al.*, 2002; Fig. 9). Fission-track data in apatites (age and track length distribution) were forward modelled with the algorithm of the AFTSolve® routine (Ketcham *et al.*, 2000) now incorporated in the latest version of the basin simulator PetroMod™ (version 9.x; www.ies.de).

Reverse-basin modelling

Inverse modelling or reverse-basin modelling in this study followed the sequence-stratigraphy concept, which considers the creation/destruction of accommodation space and its infill as the two main controls on sedimentary systems and basins. Reverse-basin modelling was carried out to

determine (1) all components of total subsidence (termed 'subsidence' in the following text) which are flexural, tectonic and compaction-induced subsidence (Fig. 11) and (2) decompacted sediment flux rates in time. These two datasets are essential input parameters for the subsequent forward modelling of the sedimentary system where sedimentation rates are fine-tuned.

Input parameters for the inverse modelling are lithology (initial porosity; after Bowman & Vail, 1999), geometries (measured and projected bed thicknesses), palaeowater depth (derived from facies analysis) and crustal parameters (e.g. effective elastic thickness T_e , plate-end-boundary distance and density of the mantle). Sea-level oscillations were initially applied during the inverse modelling (second-order sea-level curve after Hardenbol *et al.* (1998) recalibrated to the timescale used in this study) but this frequency proved to be too low especially for the studied interval of platform growth at Rosengarten (5.8 Myr; Fig. 3 and Table 1) and was subsequently

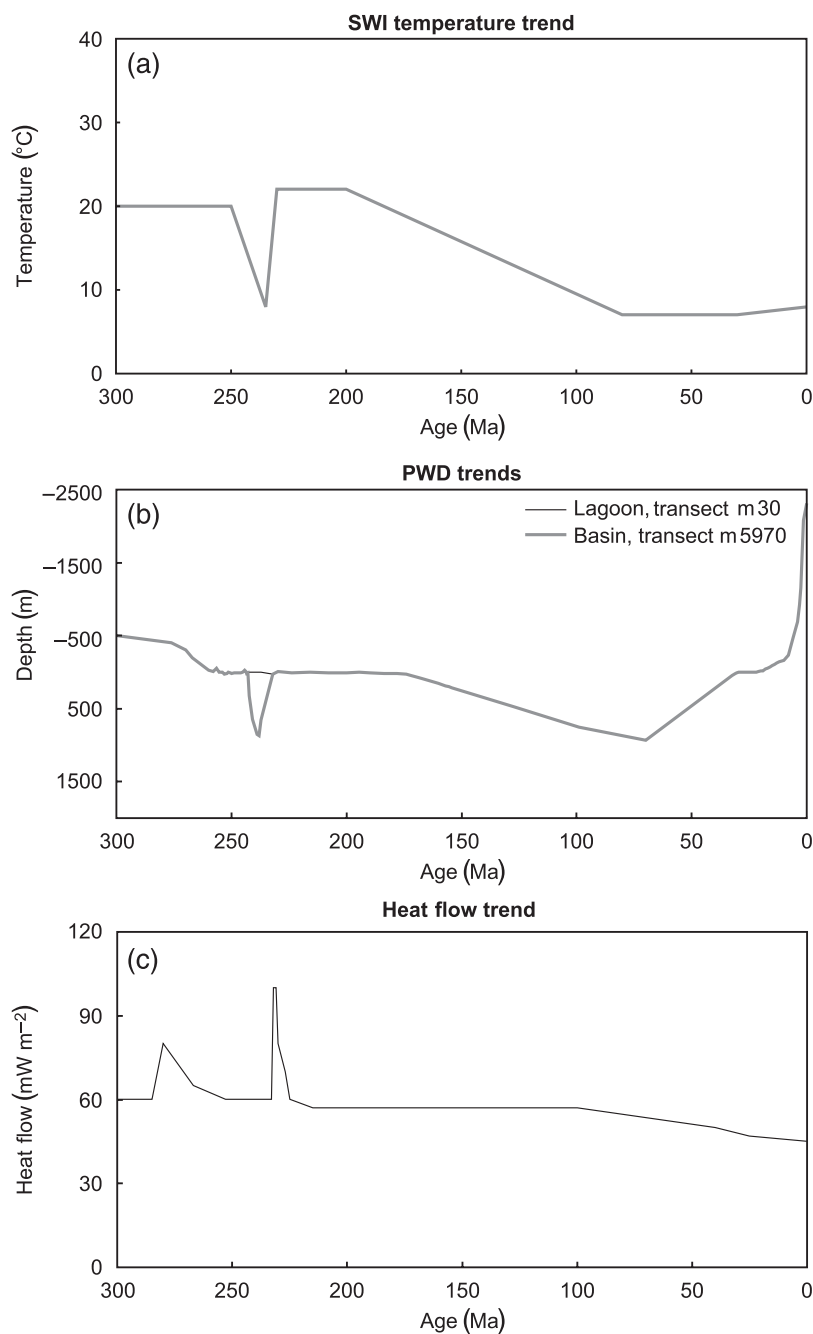


Fig. 8. Input data for thermal modelling. (a) Temperatures at the sediment-water interface (i.e., sea bottom) in time. (b) Palaeowater depth (PWD) of sea bottom in time as applied during modelling with PetroModTM and PhilTM. The two curves show PWD trends for locations of a proximal lagoon (i.e. transect metre 30) and a distal slope setting (i.e. transect metre 5970). The curve measured at a proximal location runs exactly parallel to the curve measured at a distal location apart from the time when the basin deepens (i.e., the lagoonal curve remains at constant water depths). (c) Heat-flow history as applied during modelling with PetroModTM.

neglected during further modelling runs. Third-order sea-level oscillations have not been considered because their timing and amplitude in the latest Anisian/earliest Ladinian is controversially discussed in the literature (Rüffer & Zühlke, 1995; Gianolla & Jacquin, 1998). Hence, eventual accommodation changes related to sea-level oscillations are incorporated within the calculated subsidence rates. Owing to the shortness of the transect (approximately 6 km) and the

rigidity of the underlying rheological basement (2000–2500 m thick Permian AVC), crustal parameters and flexural subsidence play a minor role. Nevertheless, recent data on the effective elastic thickness (T_e of approximately 20 km) of the lithosphere of the Venetian basin (Barbieri *et al.*, 2004) were applied (Table 3).

Subsidence component, accommodation and sediment-flux histories were calculated for each of the timesteps identified in the Permian to

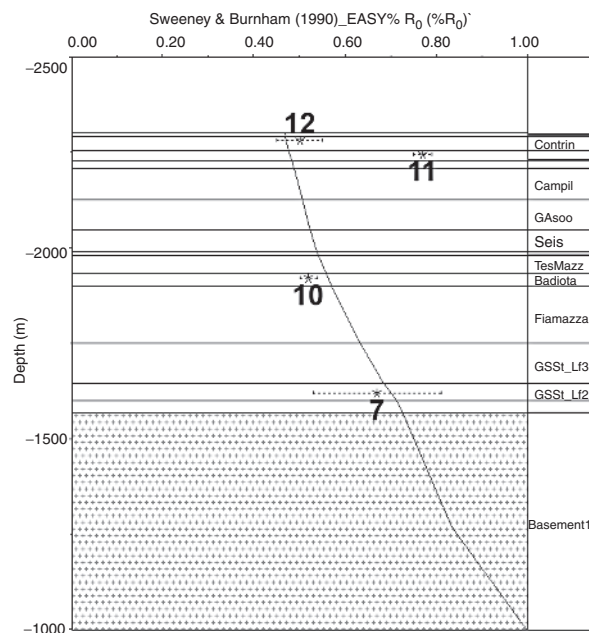


Fig. 9. Calibration of the subsidence and thermal history at Rosengarten with measured VR_r values. x-axis, vitrinite reflectance in EASY% VR_0 ; y-axis, depth in metres (negative values indicate an elevation above present-day sea level). Formations are indicated at the right-hand side. The asterisks reflect measured values, the numbers correspond to sample locations (see Fig. 4 and Table 2). The curve illustrates the calculated maturity values of the present-day situation at Rosengarten. The maturity vs. depth curve was extracted from the southern part of the transect, i.e., the part where the density of calibration parameters is at a maximum.

Late Triassic basin fill (Table 1). Basin reverse modelling runs in the opposite direction of sedimentation: the process starts at time t_2 and runs backwards in time to t_0 when all sediment layers have subsequently been removed ('backstripped'). Each timestep (t_0 , t_1 , t_2) is characterized by a distinct vector of tectonic subsidence (TS_0 to TS_2), flexural and compaction-induced subsidence as well as a change in palaeowater depth (PWD_0 to PWD_2). During each step of removal, the hypothetical depth of the basin floor is calculated without being loaded and the current depositional surface is adjusted to predefined palaeobathymetry (Fig. 11). Rates are calculated for each time layer after the removal of flexural loading effects, changes in palaeobathymetry, changes in sea level and compaction. The flexural backstripping procedure applied in the reverse-basin modelling of this study is based on the equations introduced by Turcotte & Schubert (1982, 2002) and Dickinson *et al.* (1987). The backstripping procedure with

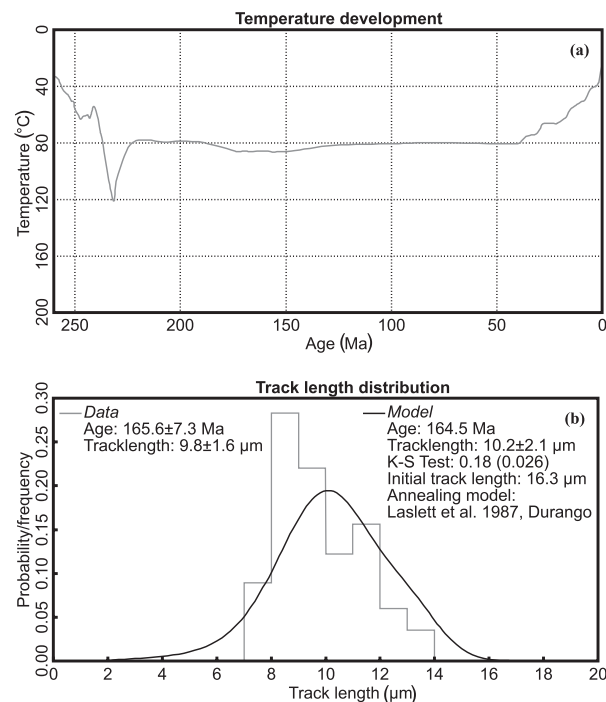


Fig. 10. Calibration of the subsidence and thermal history at Rosengarten with measured apatite-fission-track data. (a) Calculated time-temperature path at Rosengarten as derived from PetroModTM. x-axis, age in million years; y-axis, temperature in degrees Celsius. (b) Comparison of calculated with measured apatite fission tracks. Data values in grey, calculated values in black.

the applied software – PHILTM (Marco Polo Software Inc., Houston, USA) – is also described by Bowman & Vail (1999).

Sequence-stratigraphic forward modelling

Stratigraphic forward modelling in this project was mainly used to quantify carbonate accumulation rates. The simulation of facies patterns and the identification of processes operating on the platform slope were a minor goal, as well as the determination of siliciclastic sedimentation rates in the Wuchiapingian to Anisian formations. Therefore this chapter – as well as the entire study – focuses on the methodology of simulating carbonate sediments. Input parameters for sequence-stratigraphic forward modelling were tectonic subsidence, sediment parameters (Fig. 12 and Table 4) and depth-dependant carbonate-accumulation rates ('carbonate-production curve'; Fig. 13). As published by Bowman & Vail (1999), PHILTM 'represents the carbonate production

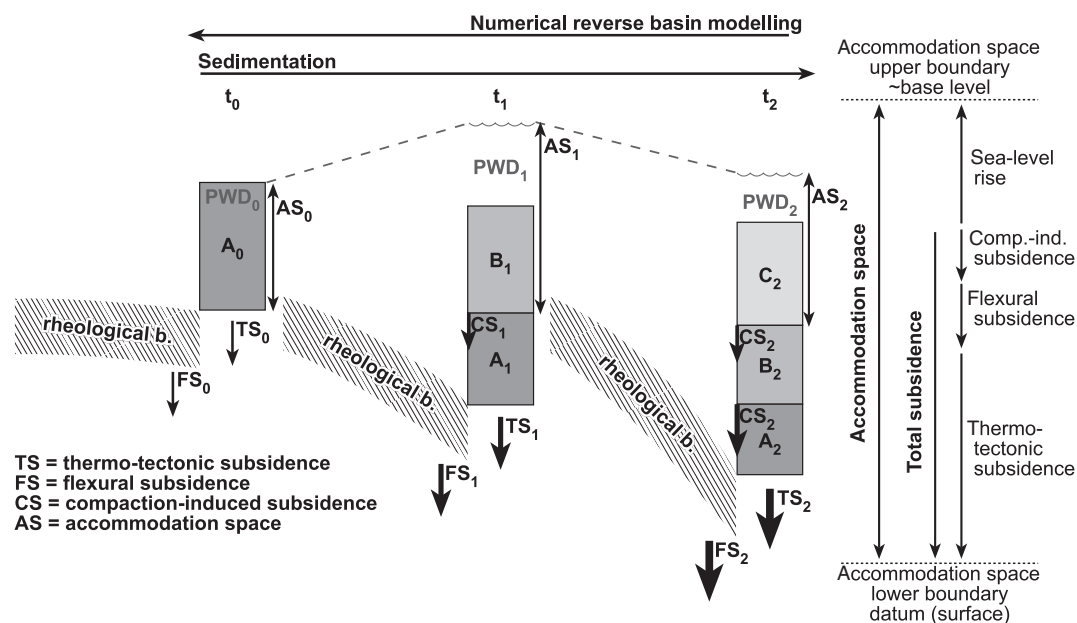


Fig. 11. Sketch illustrating the basin reverse modelling process ('backstripping'). x-axis, time; y-axis, burial depth; stratigraphic units are marked by letters A to C and different greyscales; arrows below the stratigraphic columns illustrate vectors of tectonic and flexural subsidence (thick arrow, high subsidence; thin arrow, low subsidence). The principle of development of accommodation space is illustrated on the right. Numerical values used for the flexural modelling process are shown in Table 3.

system with four water-depth-dependant functions' (Fig. 13) 'including (1) coarse-grained traction-load production composed of a laterally unrestricted factory and a laterally restricted shelf-margin factory, and (2) fine-grained suspension-load production composed of an unrestricted fine-grained factory and a pelagic factory'. However, as redeposition is included in the 'production' *sensu* Bowman & Vail (1999), the modelled rates reflect accumulation rates, not production rates. We therefore prefer to use the term accumulation rate *sensu* Bosscher & Schlager (1993). The carbonate accumulation functions used in PHILTM (Bowman & Vail, 1999: 'productivity functions') are normal distribution curves with a specified width and a maximum accumulation at a specified bathymetry (Fig. 13). Unrestricted traction and fine-grained accumulation will occur on any surface below sea level. Shelf-margin accumulation is centred about an optimal location for accumulation with respect to the open basin and exponentially reduced as a function of distance from that location by a specified factor:

$$A_{\text{depth}} = M \cdot t \cdot R \cdot e^{-(B-D_{\text{ma}})^2/W^2}$$

where A_{depth} is the accumulation for a cell during the time increment (*sensu* Bosscher & Schlager,

1993), M is the maximum accumulation rate (in m Myr^{-1}), t is time (in Myr), R is a siliciclastic reduction factor, B is the bathymetry (in m), D_{ma} is the maximum accumulation bathymetry and W the width of the productivity function (in m; after Bowman & Vail, 1999).

Sediment parameters and sedimentation/accumulation rates were adjusted in an iterative process within a geologically reasonable range and in accordance with measured data (Table 4) until a match with present-day geometries was achieved. During this iterative course of forward modelling, a sensitivity analysis was carried out in order to determine the influence of different carbonate-specific sedimentation parameters. Bowman & Vail (1999) have described in further detail the stratigraphic forward modelling process with PHILTM.

RESULTS

Thermal modelling

The combination of vitrinite reflectance recording the maximum temperatures during basin evolution and fission-track data in apatites recording the temporal development of heating and cooling enabled a highly fine-tuned thermal model of the

Table 3. Input parameters for flexural inverse modelling.

Sediment type	Sedimentary parameters	Ranges in	
		Bowman & Vail (1999)	This study
Siliciclastics	Fluvial plain gradient	0.001–0.00001	0.001
	Coastal plain gradient	0.0–0.00001	0.00001
	Shoreface gradient	0.01–0.001	0.008
	Depositional front gradient	0.1–0.01	0.08
	Coastal plain width	0–200 km	20 km
	Rollover width	1–5 km	3 km
	Depth of offlap break	10–20 m	10 m
	Barrier island height	0–10 m	0.1 m
	Barrier island width	0–15 km	2 km
	Depth of fairweather wave base	5–20 m	10 m
	Prodelta suspension distance	5–100 km	15 km
	Suspension mixing depth limit	1–200 m	5 m
	Traction fraction	0–100%	100%
	Coarse sand fraction	0–100%	10%
	Carbonates	Sabkha gradient	0.0–0.00001
Tidal flat gradient		0.0001–0.0006	0.001
Tidal range		0–15 m	1 m
Lagoon gradient			0.01
Back-reef gradient		0.1–0.001	0.02
Depth of reef crest		1–20 m	10 m
Width of margin production		0.1–5.0 km	0.2 km
Rollover width		0.5–3.0 km	1.55 km
Slope gradient		0.01–1.1	0.7 (35°)
Suspension distance of lagoonal fine-grained carbonates		1–50 km	0.1 km
Maximum suspension depth of fine-grained carbonates		3–40 m	3 m
Siliciclastic damping limit		1–150 m Myr ⁻¹	1 m Myr ⁻¹
Production time increment	0.001–0.025 Myr	0.001 Myr	
Gravity flow	Minimum bathymetric relief	100–400 m	8 m
	Slope-fan threshold depth	0–30 m	30 m
	Basin-floor fan gradient	0.001–0.0001	0.001
	Slope-fan gradient	0.03–0.001	0.001
	Relative water-level trigger factor	0 to –30 m Myr ⁻¹	–10 m
	Turbidite volume factor	0–1	1

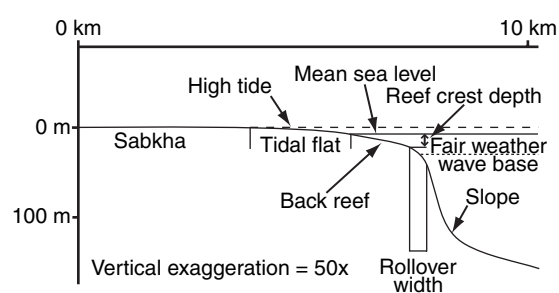


Fig. 12. Sketch illustrating the depositional environments and parameters used during the forward-modelling procedure of PHIL™ (modified after Bowman & Vail, 1999). Numerical values of the input parameters in Table 4.

Table 4. Input parameters for sequence-stratigraphic forward modelling.

Flexural parameters	This study
Flexural wavelength (km)	55.0
Effective elastic thickness (km)	20.2
Mantle density (kg m ⁻³)	3340.0
Water density (kg m ⁻³)	1030.0
Left taper limit (km)	50.0
Right taper limit (km)	500.0

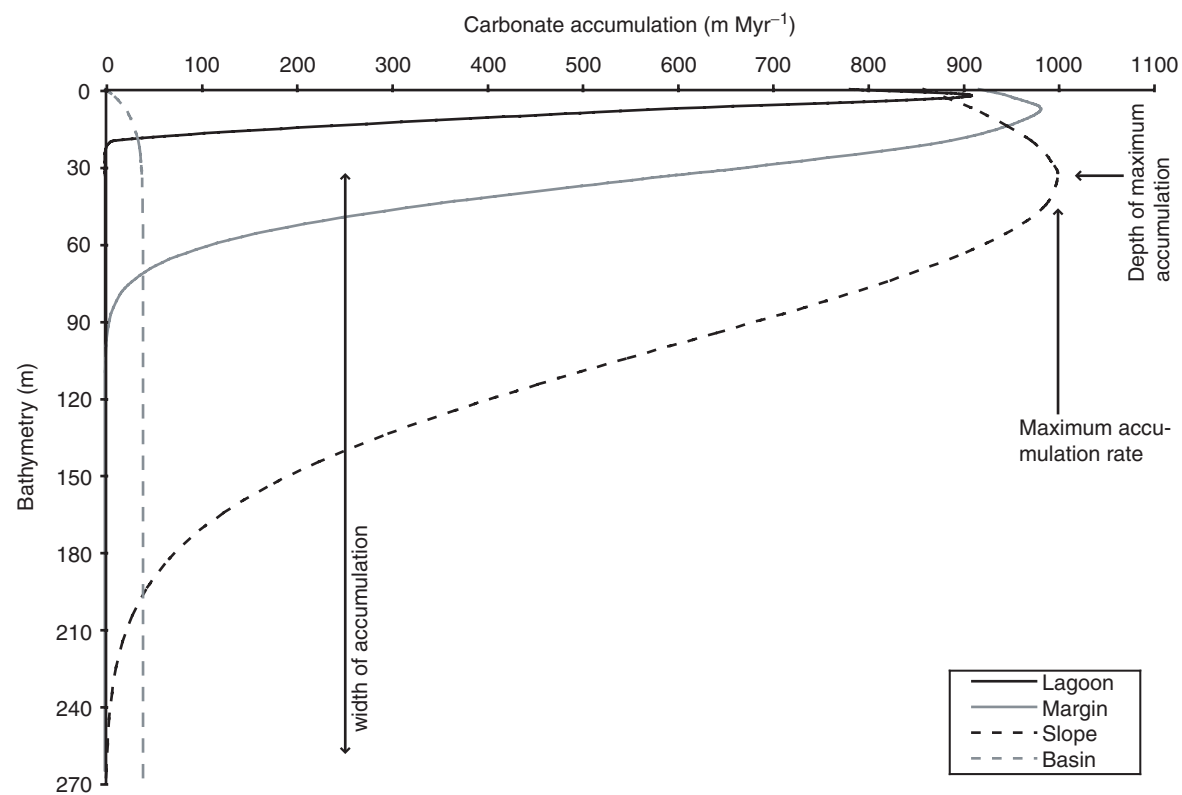


Fig. 13. Carbonate-production rates as a function of water depth during simulation with PHILTM. x-axis, carbonate-production rates in m Myr^{-1} ; y-axis, water depth in metres. Legend to functions to the bottom right. The most important variables (depth, maximum and width of production) used in the carbonate-productivity functions of PHILTM (Bowman & Vail, 1999) are indicated for the slope function (dashed black line). In order to reproduce present-day geometries, the production of the carbonate factory had to be set to values between 900 and 1000 m Myr^{-1} . Production increases from periplatform environments (900 m Myr^{-1}) across the margin (950 m Myr^{-1}) to the slope (1000 m Myr^{-1}). Pelagic production (i.e., Buchenstein Fm) was limited to 50 m Myr^{-1} .

southwest Dolomites. Modelling was stopped at a deviation of less than 5% with respect to the calibration data. In other words, the difference between iterative changes of input parameters such as: (1) the magnitude and timing of heating or cooling; (2) changes in sediment–water–interface temperatures; and (3) overall stratigraphic thickness was less than 0.3%.

Time–temperature history

A constant heat flow of around 60 mW m^{-2} is a typical value for continental crust (Allen & Allen, 1990) and hence it also was the starting point of this numerical simulation. However, after numerous runs of iteratively calibrated geohistory simulation it turned out that two intervals of elevated basal heat flow (Fig. 8c) are required in this part of the southwest Dolomites in order to match measured apatite fission-track data (Fig. 10). The first

interval between 285 and 253 Ma corresponds to the generation, extrusion and cooling of the Permian Atesina Volcanic Complex (AVC); the second interval between 233 and 225 Ma corresponds to a time when strong hydrothermal activities are recorded in the Val di Fassa area. This modelling result is in accordance with suggestions by Greber *et al.* (1997), who proposed that heat flow reached its peak (90 mW m^{-2}) at 236 Ma when an intrusion of pegmatites and an appearance of tuffs and localized lava flows are observed across the central Southalpine domain. This is also backed up by Bertotti *et al.* (1997, 1999) but with different estimates for time and extent of the elevated basal heat flow. All aforementioned authors concluded that the heat flow decreased to values of approximately 70 mW m^{-2} by 220 Ma. In contrast, Zattin *et al.* (2006) suggested that heat flow remained at high values until the end of Jurassic rifting. We believe that the observations of Barth *et al.* (1993, 1994) – a

hydrothermal event in the Val di Fassa area resetting isotopic clocks at around 230–225 Ma – much better reflects the thermal evolution in our study area. The time interval between ~100 Ma until today is characterized by a slowly decreasing basal heat flow down to values of 45 mW m^{-2} , as for example measured in wells in the Belluno basin (Sedico-1; Zattin *et al.*, 2006).

Thermal modelling indicates that maximum thermal maturity is reached during the Late Triassic (at the beginning of stage 4 in Fig. 14a and in Fig. 15b) shortly after the temperature anomaly during the extrusion of the Wengen Group volcanics (around 230 Ma; Fig. 14b) rather than during maximum burial (Fig. 15c). Formation temperatures return to background levels ~220 Ma and even seem to display a slightly negative anomaly (Fig. 14b). Thermal maturity remains unchanged up to the present day as the strata remain in the same temperature regime (Figs 14a and 15c and d); in other words, formation temperatures are constant despite increasing burial to deep-sea settings at the end of the Cretaceous (stage 4, Fig. 14b). Formation temperatures do not decrease during continent–continent collision (stage 5, Fig. 14b) and drop only as the Dolomites are exhumed to a subtle foreland-basin setting (stage 6, Fig. 14b). Fast exhumation to present-day settings decreases formation temperatures rapidly (stage 7, Fig. 14b).

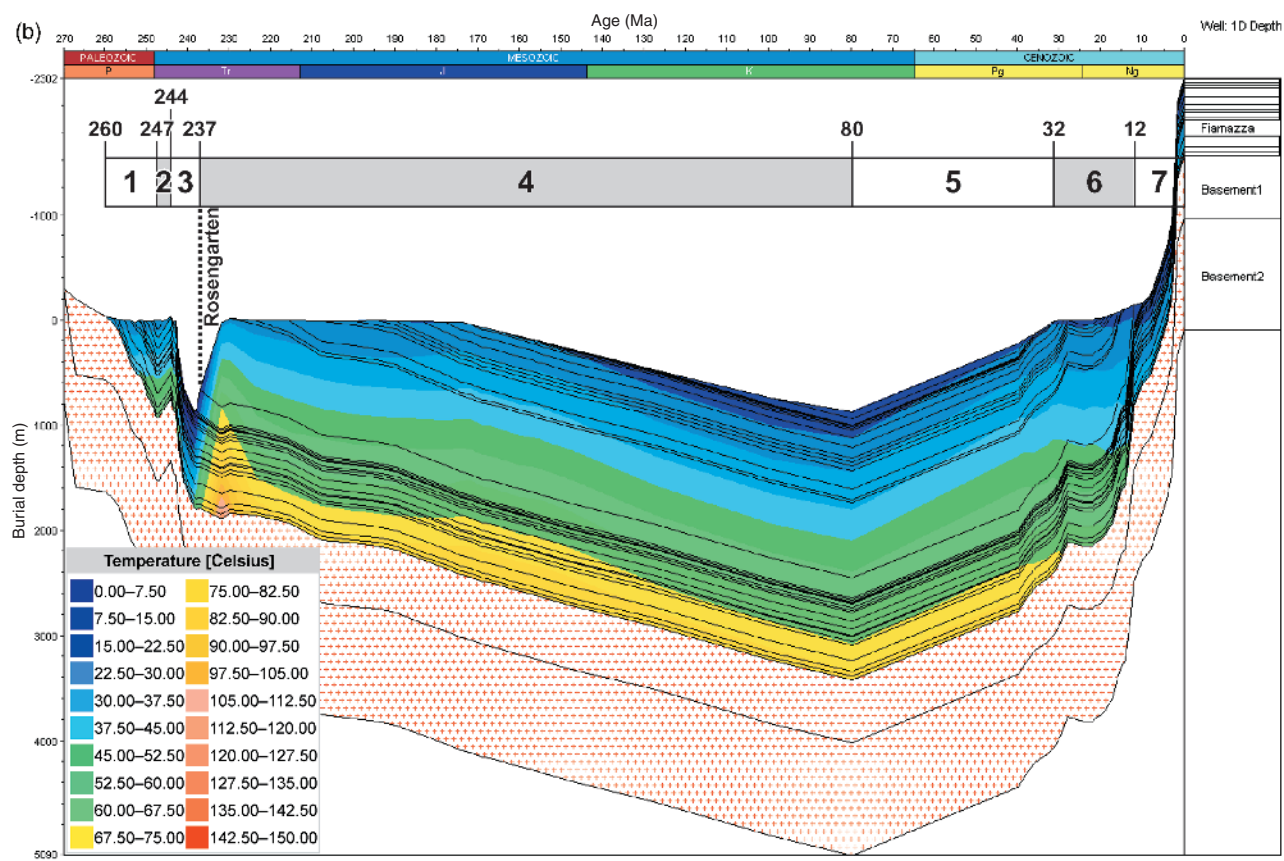
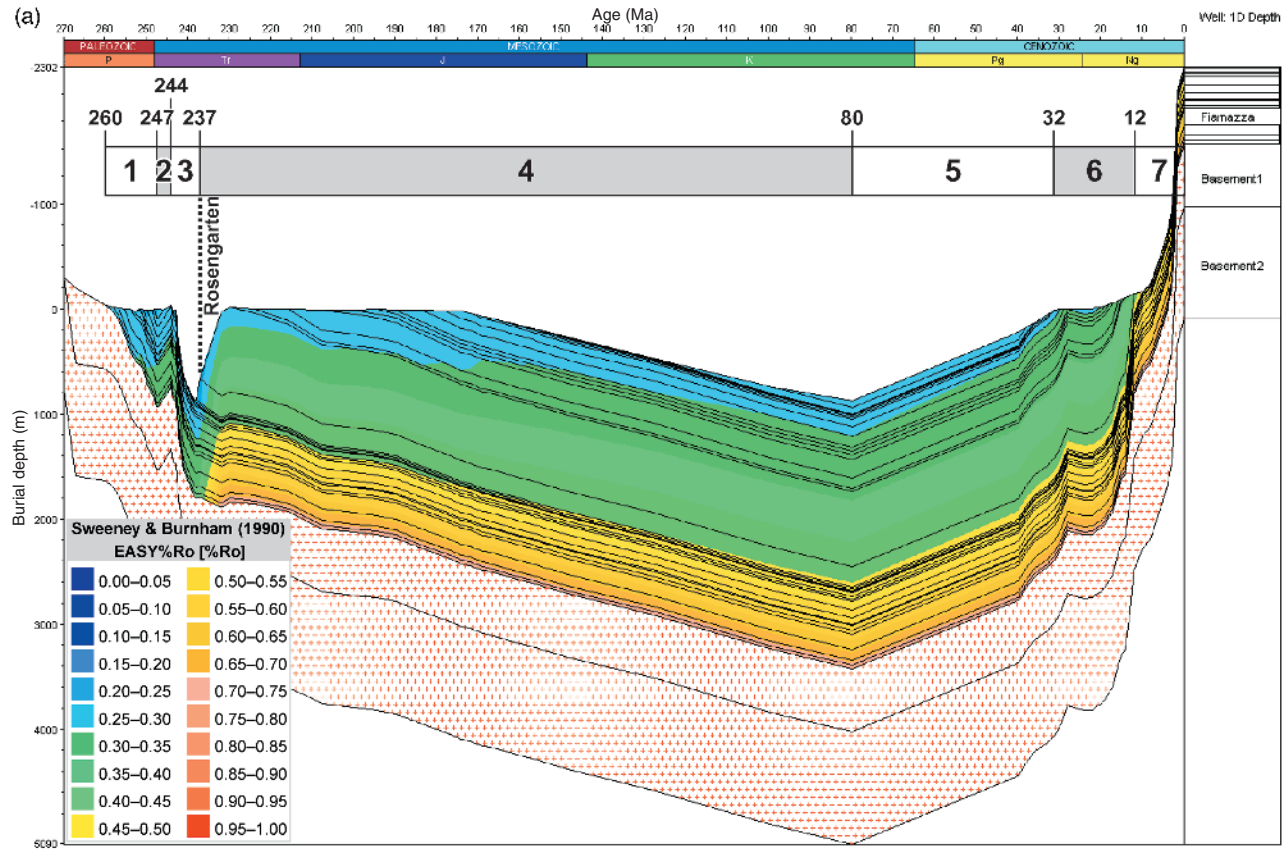
Basin geohistory

Sedimentation on the exposed basement starts at around 260 Ma (Table 1 and Fig. 14), leading to a continuous subsidence to depths at the top basement of about 800 m (stage 1 in Fig. 14). Uplift in the southwest Dolomites triggers sub-aerial erosion during stage 2 and the subsequent development of the Anisian unconformity (Fig. 14). The third stage (Fig. 14) is characterized by rapid subsidence until Middle/Late Triassic times; this episode corresponds to the accumulation of the Schlern Dolomite Fm 1 carbonate platform. The top of the youngest strata preserved at Rosengarten is indicated by the dashed line in Fig. 14. The thick sedimentary package deposited directly afterwards represents the airborne and submarine volcanoclastics of the Wengen Fm.

In order to keep platform tops and basin floors horizontal and to maintain a common gradient of slope deposits throughout all growth stages (Fig. 16), water-depth maps of more than 800 m in the deepest settings had to be applied. These

palaeobathymetric values are in accordance with assumptions from Bosellini & Stefani (1991) and Brack & Rieber (1993). Compaction of strata underneath the Rosengarten platform moves basinward together with its prograding carbonate slope, reducing porosity by its overburden (Fig. 16a–f; cf. Hunt & Fitchen, 1999; Permian Delaware and Midlands basins, USA). Highest porosities are preserved where the overlying sediments are at a minimum until the extrusion of the Wengen Group fills the basins (Fig. 16g). This interval is followed by a long period of steady subsidence (formation of the Trento platform, stage 4 in Fig. 14). Maximum thermal maturity of the transect is reached during Late Triassic times when basal heat flow is at a maximum (Figs 14a and 15a,b). The subsequent burial and subsidence of the Trento platform to deep-marine environments does not increase the thermal maturity significantly as heat flow diminishes during this period (Figs 8c and 15b,c). Maximum burial of the succession is reached during Late Cretaceous time (80 Ma; Fig. 14) when the polarity of the tectonic regime changes from extension to compression (Hsü, 1989; Dercourt *et al.*, 2000). Continuous uplift until about 32 Ma (stage 5 in Fig. 14, corresponding temperatures in Fig. 10a) followed by subaerial exposure and erosion of the youngest strata of the succession allows for a cooling of the basal strata below 80°C as required by the FT data (stage 6 in Fig. 14). Deposition of late Oligocene conglomerates (Monte Parei Fm, stage 6 in Fig. 14) leads to short-lived subsidence until major uplift occurs from 12 Ma onward (stage 7 in Fig. 14).

Another important result of thermal modelling is the quantification of eroded thicknesses above the present-day stratigraphy. The integrated modelling approach constrains the overburden to less than 1100 m (see bed thicknesses in Table 1). Both thermal maturity and apatite fission-track data clearly rule out a thick Mesozoic and Cenozoic sedimentary cover, which is also supported by recent studies on the burial history of the Trento platform (Zattin *et al.*, 2006). This furthermore confirms that there is no extensive Miocene cover during a flysch or foreland basin stadium as postulated by studies from other basins in the Alps (Venetian basin; Massari *et al.*, 1986; Eastern Alps: Winkler, 1988). The VR_f values from Permian sandstones in our study area are too low (Table 2) and the forward-modelled fission-track ages and t – T development (Fig. 10) indicate temperatures of around 80°C from 220 to 40 Ma and $<80^\circ\text{C}$ in the Permian succession since 40 Ma. The latter feature points to



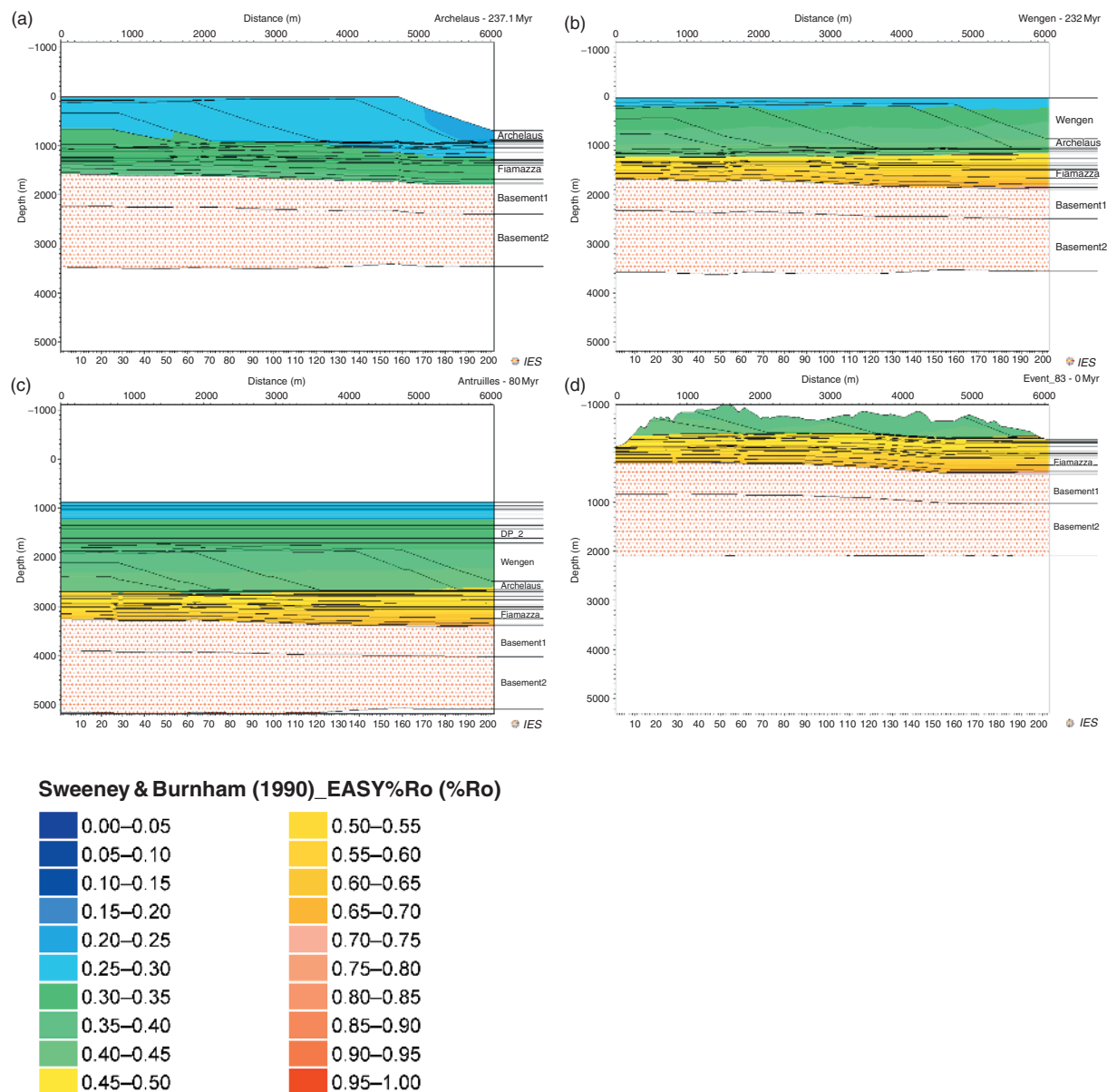
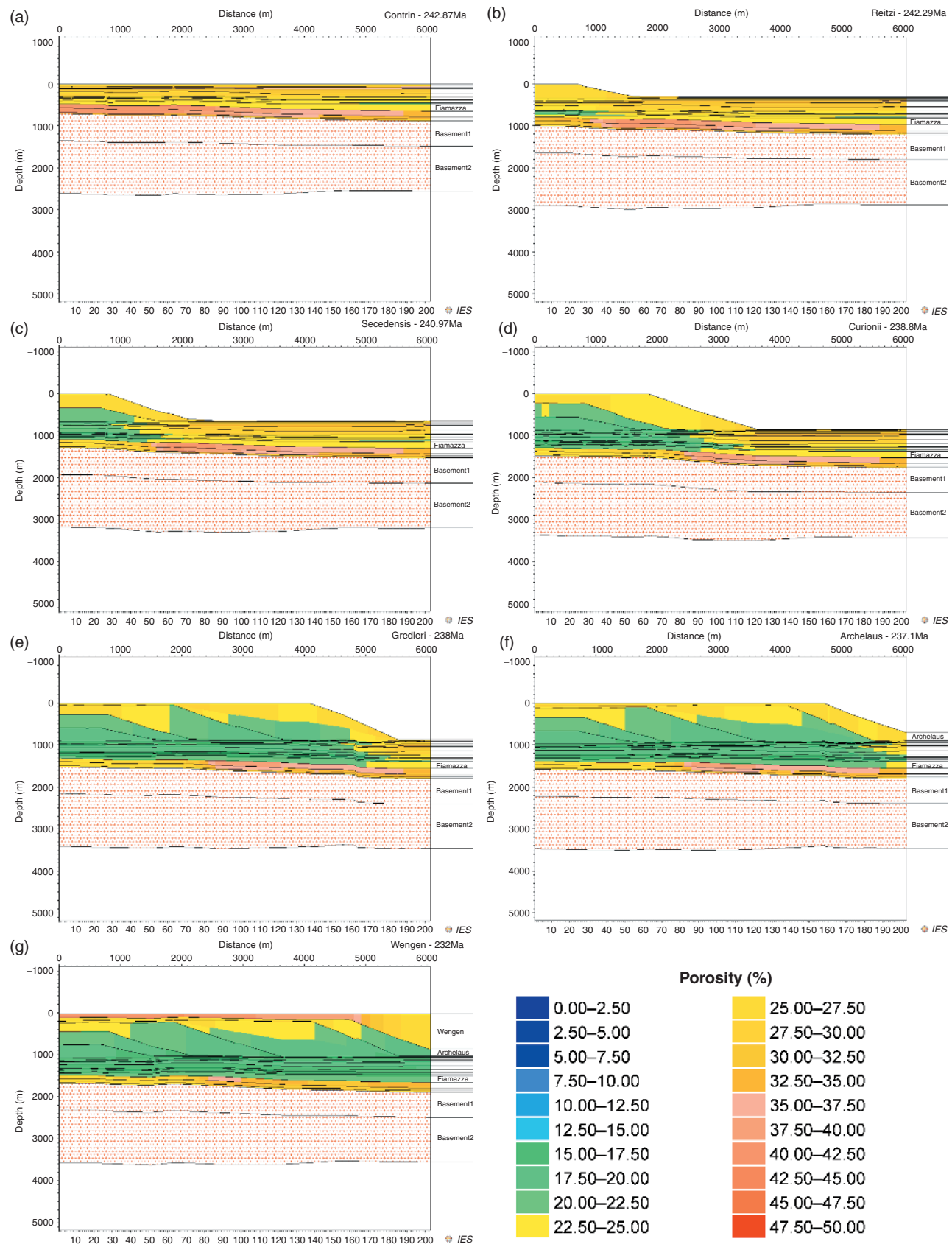


Fig. 15. Basin evolution at Rosengarten (PetroMod™). x-axis, distance along the transect in metres; y-axis, depth/elevation in metres; formations are indicated at the right-hand side; name and age of timestep in the upper right corner. Vertically exaggerated. Overlay: calculated maturity values (%VR_r), legend to the lower left. Increasing temperature during burial and rising basal heat flow create higher thermal maturity preserved until today. Fig. (d) shows the present-day situation where maximum thermal maturity is recorded by organic matter in coarse- to medium-grained sandstones of the Permian Gröden Fm (see Table 1). (a) Timestep after *Archelaus* biozone (Middle Triassic), i.e., after the last stage of platform progradation. (b) Timestep after deposition of the Wengen Fm (Middle Triassic), i.e., after maximum heating. (c) Timestep after deposition of the Antruilles Fm (Upper Cretaceous), i.e., after maximum burial. (d) Present-day situation.

Fig. 14. (Opposite page) Burial history of a pseudo well through the Rosengarten transect as calculated by PetroMod™; same location as the calibration plot in Fig. 9. x-axis, age in Ma (abbreviations: P, Permian; Tr, Triassic; K, Cretaceous; Pg, Paleogene; Ng, Neogene); y-axis, burial depth in metres; black lines are boundaries of formations and their subdivisions. Bar at the top (numbers 1–7) indicates the main stages of basin evolution with their corresponding ages. The top of the preserved stratigraphy at Rosengarten is indicated by a dashed line. (a) Overlay: calculated vitrinite reflectance (%VR_r) indicating the thermal history (legend/colour code to the lower left) of the basin. (b) Overlay: calculated temperature (°C) indicating the thermal history (legend/colour code to the lower left) of the section at Rosengarten.



a rapid uplift and exhumation of the succession as observed in other areas of the Alps and their surroundings – whether steady state or episodic (Bernet *et al.*, 2001; Carrapa *et al.*, 2003; Zattin *et al.*, 2003; Bertotti *et al.*, 2006).

Basin reverse modelling

The basin reverse modelling routine of PHIL™ (Fig. 11) calculates subsidence rates for every grid point along the transect. Two sets of subsidence rates are presented in Fig. 17, one set is derived from a proximal location within the platform interior (transect metre 30) and another one from a distal location in the basin (transect metre 5970). Owing to the rigidity of the underlying Permian AVC (>2000 m thickness) and the shortness of the transect (<10 km length), there are no distinct differences in flexural subsidence between a proximal and a distal setting. Differences in subsidence in the beginning of basin evolution – during late Wuchiapingian (uppermost part of the Gröden Fm and Fiamazza Member of the Bellerophon Fm) and late Scythian (Seis Mbr of the Werfen Fm) times – are attributed to lateral changes in bed thickness owing to relative movements along small faults. The differences in subsidence between a distal and proximal setting on the transect during late Anisian/early Ladinian times (Schlern Dolomite Fm 1, *Reitzi* and *Secedensis* biozone) originate mainly from differences in compaction-induced subsidence as larger amounts of carbonate sediment are accommodated in a proximal, lagoonal realm. As this paper focuses on the Anisian–Ladinian platform evolution, a detailed description of the pre-Anisian subsidence history is omitted for clarity.

Anisian to Late Triassic subsidence rates

Subsidence commenced with the deposition of the Richthofen Fm (conglomerates and evaporites) and increased during Morbiac Fm sedimentation (bituminous limestones and marls). The shallow marine carbonate ramp of the Contrin Fm represents an interval of decreasing subsidence. On top

of the Contrin Fm, a basinwide correlatable unconformity developed due to a subsidence peak with rates of up to 820 m Myr⁻¹. These values decrease significantly to 200–300 m Myr⁻¹ during the *Secedensis* biozone, before subsidence drops down to values around 130 m Myr⁻¹ (*Curionii* biozone) or less (50–60 m Myr⁻¹; *Gredleri* and *Archelaus* biozone) and eventually Wengen volcanics terminated platform growth. These high subsidence rates during the upper *Reitzi* and entire *Secedensis* biozone are responsible for the aggradational behaviour of the Rosengarten platform. As subsidence drops to 100 m Myr⁻¹, progradational patterns develop. As mentioned earlier and discussed by several authors (Blendinger, 1985; Doglioni, 1987), the study area was located near an active strike-slip fault system during most of the Mesozoic. Hence it seems likely that movements along the Cima Bocche Line/Stava Anticline triggered these temporal changes in subsidence (Emmerich *et al.*, 2005a).

Stratigraphic forward modelling

In order to adequately simulate the Rosengarten platform with a larger platform interior to the north and a larger basin to the south, the transect had to be extended by 2 km on each side. Essential results from previous modelling steps – such as tectonic subsidence rates and sediment flux (Fig. 7) – were incorporated in the input for the stratigraphic forward simulator of PHIL™. Sediment parameters and sedimentation rates were adjusted as explained earlier and discussed in Bowman & Vail (1999). Subaerial erosion was neglected during the forward simulation but carbonate redistribution to slope and basin was accounted for. Hence, the rates presented in this study correspond to best-fit accumulation rates (in the sense of calibration with the present-day outcrop). Real (i.e., fossil) accumulation rates would be higher because subaerial erosion and bioerosion have to be compensated for by carbonate production and sedimentation. However, the Anisian and Ladinian sea-level oscillations – indicated by the record in the neighbouring Latemar platform (Zühlke,

Fig. 16. (Opposite page) Modelled porosity evolution during progradation at Rosengarten (PetroMod™). x-axis, distance along the transect; y-axis, depth/elevation; overlay, porosity (%); legends bottom right. The progradation of the carbonate platform reduces porosity in the underlying strata. For further explanation refer to the text. (a) After deposition of the Contrin Fm (242.87 Ma). (b) After the *Reitzi* biozone (242.29 Ma). (c) After the *Secedensis* biozone (240.97 Ma). (d) After the *Curionii* biozone (238.80 Ma). (e) After the *Gredleri* biozone (238.00 Ma). (f) After the *Archelaus* biozone (237.10 Ma). (g) After deposition of the Wengen Fm (232.00 Ma).

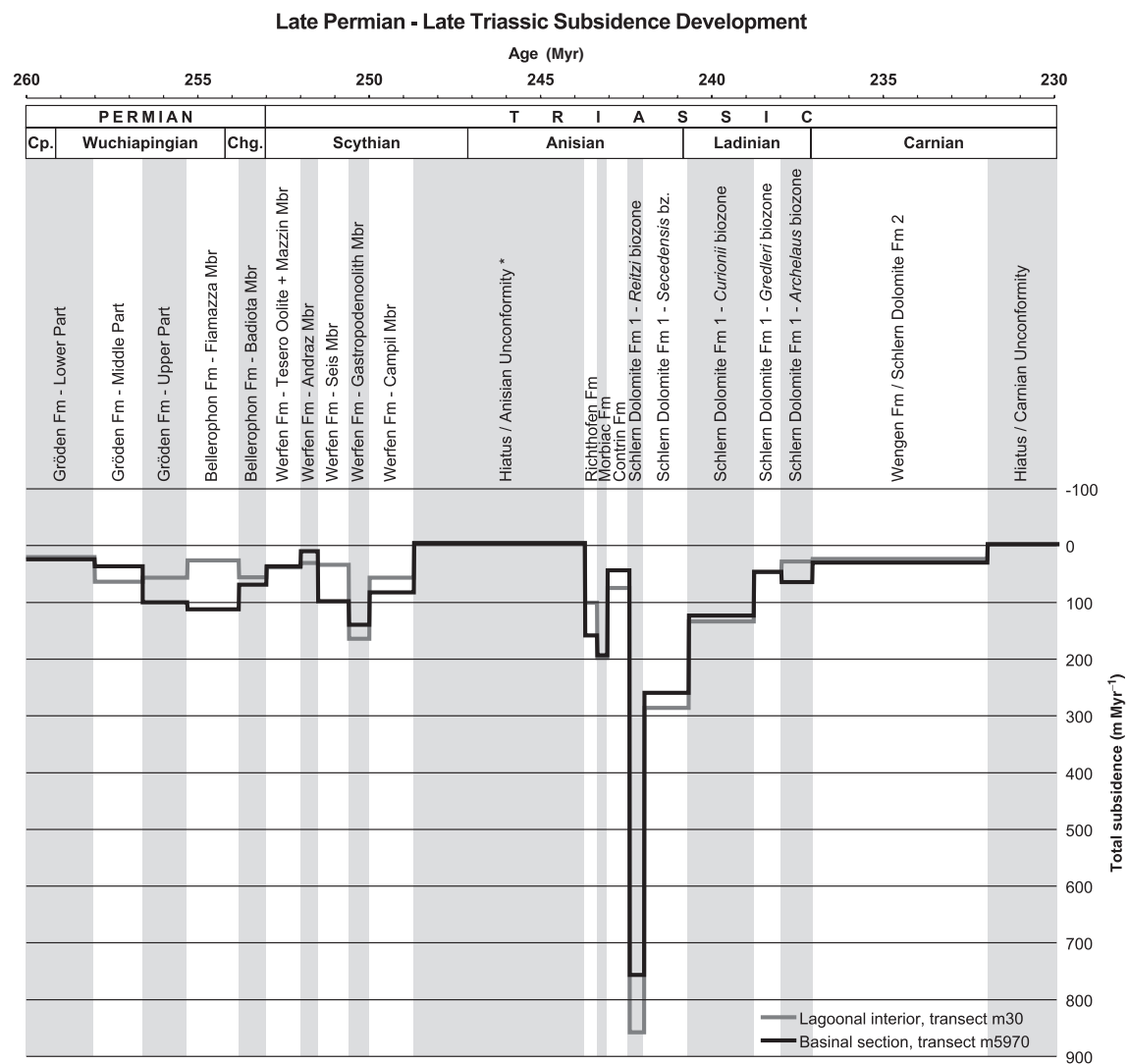


Fig. 17. Calculated total-subsidence development at the study area until the extrusion of Wengen Group volcanics (basin-reverse modelling module of PHILTM). x-axis, age in Ma; y-axis, subsidence rates in m Myr^{-1} . Subsidence was calculated at a proximal (transect metre 30; grey line) and a distal point (transect metre 5970; black line). Differences in total subsidence at proximal and distal settings are mainly attributed to differences in compaction-induced subsidence (thicker succession in distal parts). Timescale after Lehrmann *et al.* (2002), Mundil *et al.* (1996, 2001, 2003) and Yugan *et al.* (1997). Permian stages after Yugan *et al.* (1997), Triassic stages after Brack & Rieber (1993, 1994). *The backstripping process of PHILTM is not capable of calculating subsidence values of nowadays eroded formations. Therefore, the timespan of the Anisian Unconformity pictured in this figure comprises also the interval of deposition of the Val Badia and Cencenighe Members of the Werfen Fm (Table 1).

2004) – are of extraordinary high frequency and low amplitude. Therefore, the exposure time, as shown at the Latemar by dolomitic caps on top of shallowing-upward cycles (Goldhammer & Harris, 1989), of the platform top is short, and the influence of subaerial erosion can be neglected. This also implies that the carbonate factory of the platform margin and slope remains switched on during all stages of accommodation change, as seen in studies on the composition of calciturbidites

derived from Middle Triassic platforms in the Dolomites (Reijmer *et al.*, 1991; Reijmer, 1998; Maurer & Schlager, 2003; Maurer *et al.*, 2003). The influence of bioerosion is, however, difficult to quantify because it depends on many factors which are impossible to derive from the geological record. As mentioned earlier, accommodation changes are included in total subsidence rates and thus also constitute a small proportion of the forward modelled carbonate accumulation rates.

During the course of forward modelling, the entire carbonate system was set very sensitive to siliciclastic poisoning (i.e., its lower limit; Table 4) and accumulation time increments of the output files were 1 kyr (smaller time increments were limited by computing power) such that the temporal platform development could be simulated in great detail (approximately 5800 timesteps for the entire Rosengarten history).

Sensitivity analysis

A sensitivity analysis was carried out in order to quantify the influence of all input parameters (Table 4) of the PHIL™ simulator. The main results of this analysis are summarized in Fig. 18a–d. More than 1200 different runs with different numerical values of the input parameters were calculated in order to achieve a best-fit model. Among the 13 carbonate-specific ones, two parameters emerged as the most important: (1) suspension width of fine-grained carbonates and (2) rollover width (influencing the distribution of boundstone facies on the slope; for parameter definition see Fig. 12; for numerical values see Table 4). The challenge of the forward model was to match slope inclination, growth mode and distribution of boundstones on the slope. The correct pattern of aggradation followed by progradation, the extent of boundstones on the slope and the observed geometry of steep, straight to exponentially curved clinofolds was successfully modelled. This required the unique combination of rollover width set to 1.55 km and a very short suspension distance of lagoonal fine-grained carbonates of 0.1 km.

The reason why the suspension distance of fine-grained material from the platform top was set to such low values (Table 4) is the incorrect deposition of carbonate on the upper slope with higher values of the suspension distance (cf. bulge of the upper slope in Fig. 18a). This peculiar behaviour of the modelled slope system is related to the ‘carbonate productivity function’ of PHIL™ (Fig. 13) which already includes redeposition (Bowman & Vail, 1999). If the suspension distance was larger than the extent of the platform slope and all material was exported to basinal settings, progradation could not be modelled (Fig. 18b).

As discussed in the literature (Reijmer *et al.*, 1991; Blendinger, 1994; Reijmer, 1998; Kenter *et al.*, 2002, 2005; della Porta *et al.*, 2004; Seeling *et al.*, 2005), the main carbonate factory is located on the upper slope and within

water depths between 0 and 300 m. This specific, slope–productivity-driven growth characteristic is especially true for prograding carbonate platforms (Bosellini, 1989; Boni *et al.*, 1994; Seeling *et al.*, 2005). Similarly, Kenter *et al.* (2005) and della Porta *et al.* (2004) attribute the progradation of Carboniferous carbonate platforms in the Cantabrian Mountains of Spain mainly to an increased productivity of the cement-rich boundstone belt. The only possibility to simulate restricted *in situ* carbonate accumulation on the upper slope with PHIL™ is to model the shelf-margin factory, i.e., the lithology ‘boundstone’ (Bowman & Vail, 1999, p. 129). All other carbonate sediments on the slope are modelled by PHIL™ with a significant amount of allochthonous material such as lithoclastic rud- to wackestones (cf. Bowman & Vail, 1999; refer also to Section on ‘Sequence stratigraphic forward modelling’).

Best-fit model

The best-fit model is presented in Fig. 19a and b, where Fig. 19a shows the modelled transect after the last timestep of platform growth (*Archelaus* biozone, 237.10 Ma) with an overlay of lithofacies, and Fig. 19b shows the same model with an overlay of palaeobathymetry. The formations above the Permian basement and underneath the carbonate platform such as Gröden Fm (siliciclastics above the basement), Bellerophon Fm (evaporites and carbonates underneath the thin light blue line marking grainstones of the Tesero-Oolite Member at the P/T boundary), Werfen Fm (carbonates and clastics underneath the thin red line marking coarse-grained siliciclastics of the Richtigshofen Fm) and all other Anisian strata (fine-grained carbonates above the Richtigshofen Fm) are easy to discern in Fig. 19a. Formation of the Rosengarten platform post-date these Anisian strata. Platform nucleation on top of the Contrin Fm carbonate ramp occurs in response to various input parameters/boundary conditions: (1) a narrow margin combined with a restricted rollover width (Table 4); (2) higher accumulation rates on the upper slope than on the platform top (Fig. 13); and (3) subtle differences in basal topography owing to fault movement and/or lateral differences in subsidence (Fig. 19a). Minor back and forth adjustments of the margin during the first stage of platform development are attributed to difficulties of the carbonate system in establishing slope and keeping up with the rapid accommodation increase during the *Reitzi* biozone (sediment input in time is nearly outpaced

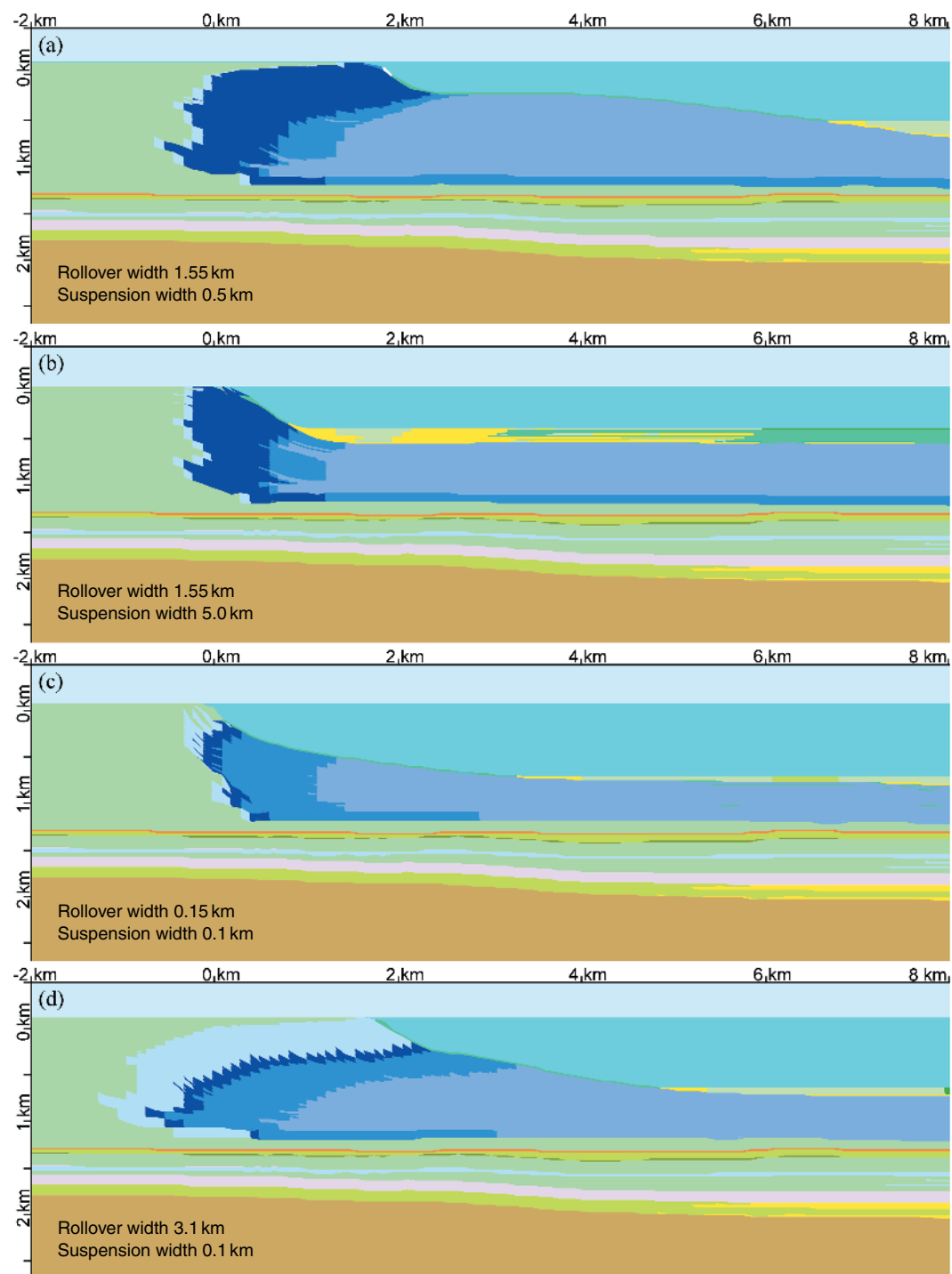


Fig. 18. Sensitivity analysis of the forward model (pictured platform development after the *Archelaus* biozone, 237.10 Ma). (a) Rollover width 1.55 km (wide boundstone belt) and suspension width 0.5 km (bulge-like deposition of fine-grained material in an intermediate position and steep proximal clinoforms) resulting in weak, late-stage progradation. (b) Rollover width 1.55 km (wide boundstone belt) and suspension width 5.0 km (deposition of fine-grained material in a distal position and steep proximal clinoforms) resulting in aggradation, late-stage progradation. (c) Rollover width 0.15 km (narrow boundstone belt) and suspension width 0.1 km (deposition of fine-grained material within the bounds of the slope and exponentially curved clinoforms) resulting in weak retrogradation. (d) Rollover width 3.1 km (wide back-reef belt and narrow boundstone belt) and suspension width 0.1 km (deposition of fine-grained material within the bounds of the slope and exponentially curved to nearly straight clinoforms) resulting in progradation. For legend see Fig. 19.

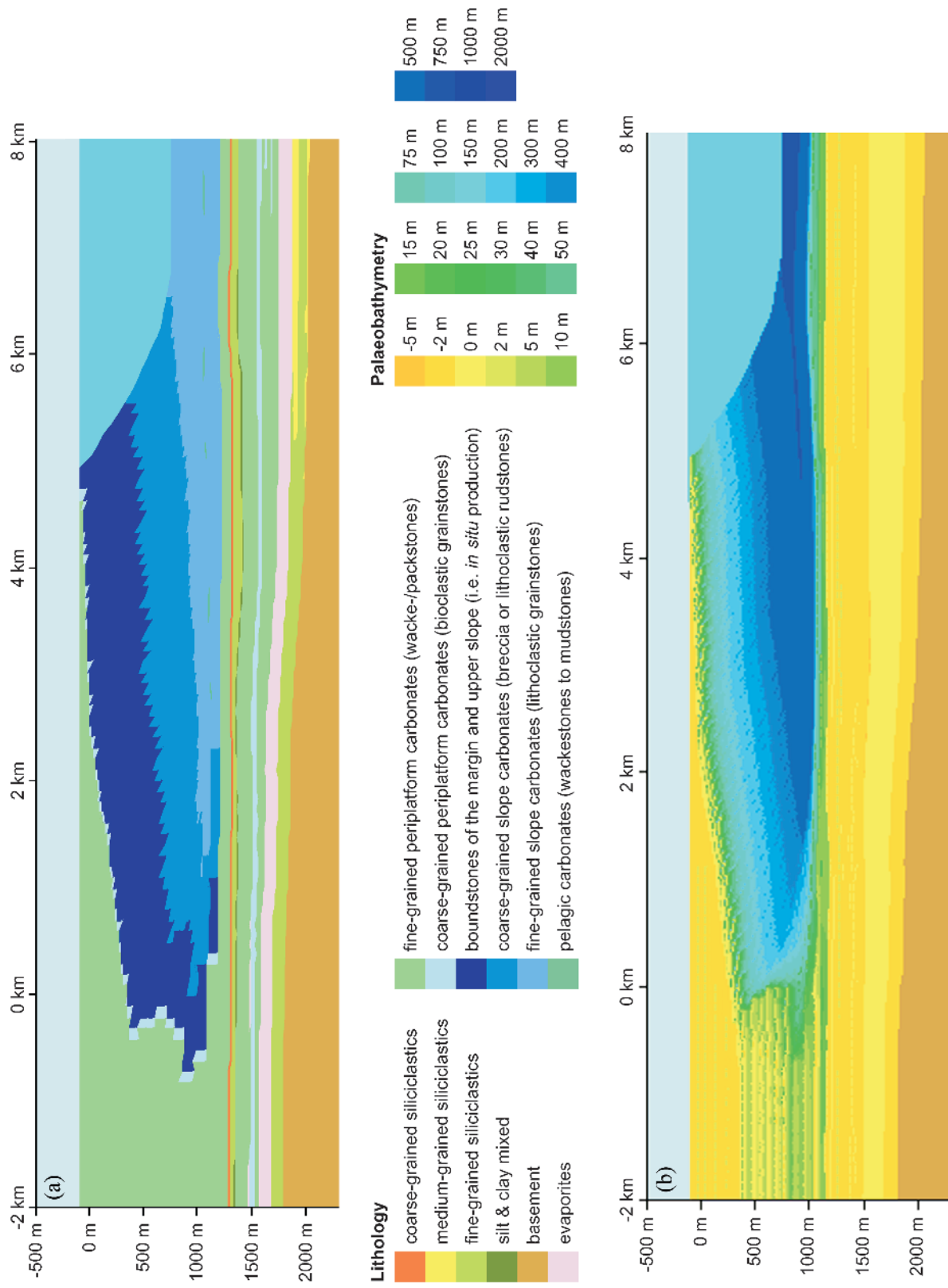


Fig. 19. Rosengarten transect as simulated with PHIL™ after the last timestep of platform progradation (*Archelais* biozone, 237.10 Ma). x-axis, distance along transect in kilometres; y-axis, elevation/depth in metres (negative values, elevation above sea level of the respective timestep; positive values, depth below sea level); no vertical exaggeration. (a) Overlay: lithologies. Owing to the similarity in grain size, fine-grained toe-of-slope deposits (Schlern Fm) have the same colour code as the fine-grained calciturbiditic deposits of the basal Buchenstein Fm. (b) Overlay: palaeobathymetry. This overlay illustrates the Anisian transgressive surface, where deep marine sediments of the Buchenstein Fm (dark blue) unconformably overlie the shallow-marine carbonate ramp of the Contrin Fm (light green).

by accommodation change, i.e., $A' \rightarrow S'$; *sensu* Seeling *et al.*, 2005). Nevertheless, the aggradation trend is clearly identifiable. The palaeowater depth overlay facilitates the recognition of this first phase and especially highlights the transgressive surface in basinal settings developed on top of the Contrin Fm (Fig. 19b).

The resulting trajectories of the margin are illustrated in Fig. 20a and b. The first stage, characterized by a steep, nearly vertical trajectory (1 in Fig. 20; the present-day situation is shown in Fig. 20c for comparison), is followed by an interval of progradation (2 in Fig. 20). The second stage – i.e., the *Curionii* biozone – is typified by a shallow to intermediate trajectory of the margin until fast progradation with very shallow trajectories occurs during the last stages (3 in Fig. 20). A comparison with the growth mode of the Rosengarten platform according to Maurer (1999, 2000) reveals almost the same arrangement of trajectories

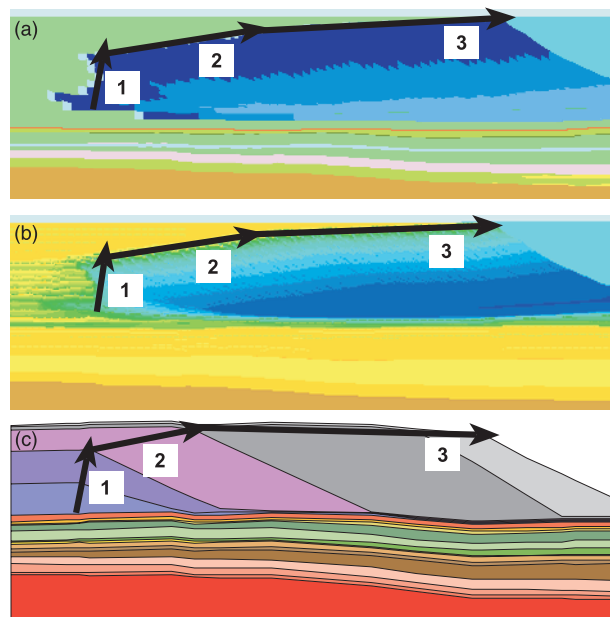


Fig. 20. Simplified comparison of the simulated transect with reality. *x*-axis, distance along transect; *y*-axis, elevation/depth; no vertical exaggeration. (a) and (b) Details from Fig. 19a (lithology) and 19b (palaeobathymetry). The three different growth stages are marked with arrows and numbers (1: aggradation during *Reitzi* and *Secedensis* biozone; 2: progradation during *Curionii* biozone; 3: rapid progradation during *Gredleri* and *Archelaus* biozone). (c) Detail from reconstructed transect after Bosellini & Stefani (1991) and Maurer (1999, 2000; Fig. 6). The three different growth stages are marked in the same way as in (a) and (b). The last stage of the platform development appears to be dipping to the right (south) owing to the post-sedimentary, fault-related dip of the underlying strata.

(Fig. 20c). In the model, the initial phase (stage 1) is a bit shorter whereas the growth stage of the *Curionii* biozone (stage 2) seems a bit longer. This indicates that the duration of the *Curionii* biozone may in reality have been shorter than modelled in this study (i.e., <2.2 Myr as derived from the chronostratigraphic data of Mundil *et al.*, 1996, 2003).

Decompacted carbonate accumulation rates without subaerial erosion and bioerosion rates but including redeposition in some facies ('production rates'; Fig. 13) increase from lagoon ('periplatform production') to slope ('platform slope production'). The growth mode of the Rosengarten platform is matched with constant accumulation rates throughout all biozones of platform growth: 900 m Myr⁻¹ was applied for periplatform accumulation, 980 m Myr⁻¹ for platform margin accumulation, 1000 m Myr⁻¹ for platform slope accumulation and 50 m Myr⁻¹ for pelagic accumulation. The width of the carbonate functions applied in the forward model corresponds to the following facts: (1) the main carbonate factory is found on the slope (Blendinger, 1994); and (2) boundstone carbonate production on the slope takes place until ~300 m water depth (della Porta *et al.*, 2004).

DISCUSSION

Burial and thermal history

Low vitrinite reflectance values together with short apatite fission tracks indicate a long, shallow burial of the Rosengarten succession until the Oligocene, followed by fast uplift/cooling (Figs 10 and 14). Values of vitrinite reflectance between 0.5% VR_r and 0.8% VR_r indicate maximum temperatures during burial of the order of 110°C. As illustrated by the burial history plot in Fig. 10b, maximum temperatures were reached by Late Triassic time when a high basal heat flow of 110 mW m⁻² was reached for a short while around 230 Ma. This was necessary in order to reproduce (1) the observed thermal maturity; and (2) the measured ages of the apatites. This elevated basal heat flow during the Late Triassic is associated with violent magmatic events in the vicinity of the Predazzo–Monzoni area. Many studies confirm this observation by either reset isotopic clocks from the Fassa Valley (Barth *et al.*, 1993, 1994) or thermal modelling of sedimentary successions in the Southern Alps (Greber *et al.*, 1997). However, our integrated 4D basin simulation contradicts the

thermal history postulated by Zattin *et al.* (2006) for the Dolomites. The raw data presented in this study as well as the modelling results show no indications for an elevated Jurassic heat-flow due to rifting as reported by Zattin *et al.* (2006).

The Late Jurassic to Cretaceous subsidence trend calculated by Winterer (1998) for the Trento platform had to be lowered by ~15%. Otherwise, the Rosengarten would have been buried too deeply and the forward modelled time–temperature history would not have matched the measured fission-track data. Uplift occurred when the polarity of plate movement was reversed (approximately 80 Ma), fast uplift prevailed from 32 Ma onward and the succession eventually moved above the 80°C isotherm. This rapid exhumation–cooling rate is confirmed by recent fission-track data of the Southern and Western Alps (Carrapa *et al.*, 2003), as well as by provenance analyses (Dunkl *et al.*, 2001; Zattin *et al.*, 2003) and apatite (U–Th)/He thermochronology (Bertotti *et al.*, 2006).

Porosity evolution

The porosity evolution of the strata underlying the carbonate platform reflects the growth mode of the Rosengarten. During the last, progradational stage of platform evolution, maximum porosities in the Permian Gröden Fm are preserved in distal, basinal areas (Fig. 15e and f). The decrease in porosity underneath the slope sediments mimics their progradation – i.e., an area of low porosity is moving basinwards propagated by compacting slope deposits. This has implications for (1) early diagenetic fluid-flow dynamics and (2) shallow siliciclastic hydrocarbon reservoirs below prograding (carbonate) slopes. Concerning (1), the migration of fluids during the earliest stages of diagenesis might thus be rather basinward than directed towards the platform owing to the pressure differences exerted by the different timing of sedimentary loading. With respect to model 2, better reservoir characteristics are subsequently preserved underneath basinal strata, not underneath carbonate platforms. However, basin infill and diagenesis during deeper burial will most probably level lateral differences in the underlying strata (Fig. 15g).

Carbonate accumulation rates

Previous studies on reef communities and carbonate platforms in the Dolomites (Fois & Gaetani, 1984; Senowbari-Daryan *et al.*, 1993) have stressed

the Anisian recovery of reef builders from the end-Permian faunal crisis when 62% of marine invertebrate families (McKinney, 1985) and up to 96% of species (Raup, 1979) were extinguished. New investigations on trace-fossil abundance in the Lower Triassic Werfen Fm (Fig. 3) demonstrate a gradual reappearance of taxa throughout the Lower Triassic of the Dolomites (Werfen Fm) and a complete recovery in the Uppermost Scythian (represented by the top of the Werfen Fm; Twitchett, 1999). In addition, palaeontological studies from other Triassic carbonate platforms around the world also indicate a fast recovery of the calcimicrobial carbonate factory (for complete discussion and references see Flügel, 2002).

These different observations are confirmed by the modelled sedimentation rates: accumulation of up to 1000 m Myr⁻¹ of carbonate sediment is necessary in order to: (1) keep-up the platform during the rising A'/S' conditions at the beginning; and (2) to simulate the fast progradation during the decreasing A'/S' conditions in the second stage of platform development (*sensu* Seeling *et al.*, 2005). The best fit with present-day geometries was achieved using a constant rate of carbonate accumulation from 900 to 1000 m Myr⁻¹, increasing from platform top to upper slope. Hence, the main *in situ* carbonate factory is located on the margin and upper slope ranging from shallow subtidal to 200–300 m water depth. This is in accordance with studies on carbonate platforms from the Upper Carboniferous of the Asturian and Cantabrian mountains in Spain (Kenter *et al.*, 2002, 2005; della Porta *et al.*, 2004) and confirmed at platforms where $A' > 0$ and $A'/S' \rightarrow 0$ (i.e., 'pathologically prograding' Bosellini, 1989; Seeling *et al.*, 2005). In the Dolomites, the studies of Keim & Schlager (2001) and Maurer *et al.* (2003) highlight the importance of the automicrite factory on the slope for the growth of Middle Triassic carbonate platforms. The boundstone facies with laterally restricted and hence *in situ* accumulation, modelled in this project, is the driving mechanism behind (1) initial platform growth and (2) late-stage progradation.

Previous studies have calculated/estimated compacted accumulation rates of 200–500 m Myr⁻¹ (Dürrenstein: Schlager, 1981; Schlager *et al.*, 1991), 600 m Myr⁻¹ (Sella: Keim & Schlager, 2001) and 800 m Myr⁻¹ (the Anisian part of the Latemar succession: Egenhoff *et al.*, 1999) for Middle to Late Triassic carbonate platforms in the Dolomites. The rates simulated during this study are higher because they represent decompacted

accumulation (up to 1000 m Myr^{-1} of accumulation in order to keep up with up to 820 m Myr^{-1} of subsidence). However, these values are within the range of the slope-shedding model of Kenter *et al.* (2005), who postulated $\sim 1000 \text{ m Myr}^{-1}$ of *in situ* boundstone growth for prograding platforms in the Carboniferous (Asturias, Spain and North Caspian Basin, Kazakhstan). This adds further evidence to observations of a rapid recovery of the carbonate factory some 10 Myr after the faunal crisis at the end of the Permian (following the timescale in Table 1). Hence, the results of our study question the hypothesis of mounded geometries owing to low carbonate productivity at the coeval but drowned Monte Cenera carbonate platform (Blendinger *et al.*, 2004). It is much more likely that the drowning is related to upwelling of cold water masses into the western Tethys as proposed by Preto *et al.* (2005) than to low productivity of a not fully recovered carbonate factory.

The difference of $80\text{--}180 \text{ m Myr}^{-1}$ between subsidence rates as determined by the basin-reverse modelling and the minimum carbonate accumulation rates as required in the stratigraphic forward modelling results for two reasons: (1) timesteps in basin-reverse modelling are much longer than in forward modelling and they thus reflect longer intermediate values ($10^6\text{--}10^5$ vs. $10^3\text{--}10^2$ years); (2) carbonate sediments are redistributed out of the transect (debris flows, calciturbidites) and subject to bioerosion and dissolution. These effects have subsequently to be added on top of the subsidence rates.

Controls on platform evolution at Rosengarten

The slope of the Rosengarten is characterized by two stages of platform evolution as recognized by Bosellini (1984), Bosellini & Stefani (1991) and Maurer (1999, 2000). The initial aggradational phase is followed by a progradational period towards the end of platform development. This study shows that a significant increase in carbonate accumulation rates during the development of the Rosengarten platform as postulated by Maurer (1999, 2000) is not necessary for the explanation of this behaviour and can most likely be ruled out as a possible explanation for the fast progradation.

- (1) The onset of platform formation occurs in the late Anisian. By this time, the carbonate factory in the Dolomites is fully recovered from the faunal crisis at the Permian–Triassic

boundary as evidenced by early Anisian reef communities (Fois & Gaetani, 1984; Senowbari-Daryan *et al.*, 1993).

- (2) The existence of the Rosengarten platform covers less than five biozones (i.e., 5.77 Myr) – an interval during which changes in intrinsic features (*sensu* Schlager, 2000; i.e., changes of the biotic and abiotic carbonate factory) are not observed on coeval platforms in the vicinity (Emmerich *et al.*, 2005b, and references therein).
- (3) According to Schlager (1999), the accumulation rate of carbonate platforms is much more likely to decrease in the million-year range due to changing environmental factors – a fact which would contradict increasing accumulation rates.
- (4) The palaeogeographical configuration of the southwest termination of the Tethys is more or less stable during the Anisian and Ladinian, there are no indications for climate changes (Dercourt *et al.*, 2000).

Therefore, temporal changes in tectonic subsidence have to be assumed as the driving force for this two-phased growth. A short-lived, pulse-like peak of up to 820 m Myr^{-1} subsidence during the *Reitzi* biozone decreased to $200\text{--}300 \text{ m Myr}^{-1}$ during the *Secedensis* biozone, resulting in an aggrading platform. As soon as the *Curionii* biozone was reached, subsidence dropped to 100 m Myr^{-1} resulting in strong progradation of the platform lasting until the termination of platform development via the extrusion of Wengen Group volcanics. Changes in wind or wave direction as the driving mechanisms behind platform progradation are considered less likely for two reasons.

- (1) This extrinsic factor must have first hindered (during the aggradational phase) and then promoted progradation of the slope. This means that environmental factors must have changed by 180° during the growth of the Rosengarten platform. This radical change is not supported by any other observations from the Dolomites (Egenhoff *et al.*, 1999).
- (2) The main carbonate factory is located on the upper slope and is especially active during progradational phases (Blendinger, 1994; Reijmer, 1998; Della Porta *et al.*, 2004; Seelinger *et al.*, 2005). This behaviour was coined ‘slope-shedding’ by Kenter *et al.* (2005).

The subsidence peak of the late *Reitzi* to early *Curionii* biozone can be observed throughout the western Dolomites (Bechstädt & Brandner, 1970; Bechstädt *et al.*, 1978; Rüffer & Zühlke, 1995) and is most probably connected with strike-slip tectonics at the transpressive–transtensive passive continental margin (Doglioni, 1983, 1984; Blendinger, 1985). As the southeast side of the Rosengarten is located very close to the Stava Line/Cima Bocche Anticline (approximately 10 km), this two-phased growth is most probably caused by tectonic movements and stillstands along this line. Sudden, in the order of 1 Myr or less, movements cause peaks in tectonic subsidence (intervals with aggradational clinofolds) whereas during times of tectonic inactivity and/or updoming of the Predazzo magmatic chambers subsidence stopped (intervals with progradational clinofolds).

CONCLUSIONS

The chosen methods of an integrated basin simulation are a prerequisite for modelling subaerially exposed sedimentary systems. The quantification of sedimentary hiatuses, erosion and burial by thermal subsidence modelling corrects for compaction and stratigraphic bias before sequence-stratigraphic modelling is realized. Integrated basin simulation must include the reconstruction of burial history. Calibration of thermal modelling with vitrinite reflectance and FT measurements revealed that Neogene flysch or molasse-type sediments above the present-day topography, as inferred for other Alpine basins (Massari *et al.*, 1986; Winkler, 1988), did not affect temperature and burial history. In other words, these foreland-basin sediments were either very thin or not present at all. The thinness of eroded stratigraphy above the Rosengarten transect contrasts with the regional coalification pattern of the eastern Dolomites (Zattin *et al.*, 2006). The higher thermal maturity in that area requires either a significantly higher heat flow or greater thicknesses of the now eroded Cretaceous to Cenozoic overburden. Whereas the latest cooling phase of the eastern Dolomites seems to be similar to that of the Rosengarten area, higher thermal maturity in the eastern and central Dolomites further highlights the importance of the Trento platform for the thermal evolution of the western Dolomites.

Owing to numerous and high-quality chrono-, bio- and cyclostratigraphic data, the Middle Triassic Rosengarten carbonate platform is an ideal area

for assessing carbonate accumulation rates after the Permian–Triassic crisis and the response of platforms to temporal changes in subsidence. An integrated approach of thermal and stratigraphic modelling reveals that the Rosengarten platform keeps up successfully with subsidence rates of up to 820 m Myr⁻¹. Both stages of platform growth – first aggradation and later progradation – originate in temporal variations in total subsidence. In the case of the Rosengarten, tectonic subsidence and its variations have been discussed as the major extrinsic (*sensu* Schlager, 2000) factors for platform and slope evolution. Other parameters such as sea-level oscillations and palaeowind or -wave directions were significantly less important and/or heavily overprinted by variations in subsidence. High-frequency sea-level oscillations as recorded by the accommodation history of the lagoonal interior at Torri del Vajolet (Fig. 5a) have not been preserved or recorded in the development of the platform slope (Harris, 1994; Reijmer, 1998; Emmerich *et al.*, 2005b). The best-fit carbonate accumulation rates of 900–1000 m Myr⁻¹ reach the values of subrecent carbonate platforms (Enos, 1991). Additionally, sequence-stratigraphic forward modelling allowed further constraints on the palaeowater depths of the Buchenstein Fm. Best-fit simulation indicates water depths of up to 800 m at the sediment–water interface of the distal succession. The key considerations of this study are: (1) the *locus* of the carbonate factory on the upper slope; (2) its high productivity after the Permian–Triassic faunal crisis; and (3) the independence of production from sea-level and ultimately accommodation change.

ACKNOWLEDGEMENTS

Axel Emmerich thanks the ‘Studienstiftung des deutschen Volkes’ (German National Academic Foundation, Bonn) and the International Postgraduate Programme (IPP, University of Heidelberg) for financial support during this study. This article benefited from thorough reviews by John Reijmer (Marseille, France), Marco Stefani (Ferrara, Italy) and Georg Warrlich (Muscat, Oman).

REFERENCES

- Allen, P.A. and Allen, J.R. (1990) *Basin Analysis, Principles and Applications*. Blackwell Science, Oxford, 451 pp.
 Aurell, M., Badenas, B., Bosence, D.W.J. and Waltham, D.A. (1998) Carbonate production and offshore transport on

- a Late Jurassic carbonate ramp (Kimmeridgian, Iberian Basin, NE Spain); evidence from outcrops and computer modelling. In: *Carbonate Ramps* (Eds V.P. Wright and T.P. Burchette), *Geol. Soc. Spec. Publ.*, **149**, 137–161.
- Barbieri, C., Bertotti, G., Di Giulio, A., Fantoni, R. and Zoetemeijer, R.** (2004) Flexural response of the Venetian foreland to the Southalpine tectonics along the TRANSALP profile. *Terra Nova*, **16**, 273–280.
- Barker, C.E. and Pawlewicz, M.J.** (1986) The correlation of vitrinite with maximum temperature in humic kerogen. In: *Paleogeothermics* (Eds G. Buntebarth and L. Stegena), pp. 79–93. Springer, New York.
- Barth, S. and Mohr, B.A.R.** (1994) Palynostratigraphically determined age of the Tregiovo sedimentary complex in relation to radiometric emplacement ages of the Atesina volcanic complex (Permian, Southern Alps, N Italy). *Neues Jb. Geol. Paläontol. Abh.*, **192**, 273–292.
- Barth, S., Oberli, F., Meier, M., Blattner, P., Bargossi, G.M. and Di Battistini, G.** (1993) The evolution of a calc-alkaline basic to silicic magma system: Geochemical and Rb–Sr, Sm–Nd and $^{18}\text{O}/^{16}\text{O}$ isotopic evidence from the Late Hercynian Atesina-Cima d’Asta volcano-plutonic complex, Northern Italy. *Geochim. Cosmochim. Acta*, **57**, 4285–4300.
- Barth, S., Oberli, F. and Meier, M.** (1994) Th–Pb versus U–Pb isotope systematics in allanite from co-genetic rhyolite and granodiorite: Implications for geochronology. *Earth Planet. Sci. Lett.*, **124**, 149–159.
- Bechstädt, T. and Brandner, R.** (1970) Das Anis zwischen St. Vigil und dem Höhlensteintal (Prager und Olinger Dolomiten, Südtirol). *Festband Geol. Inst., 300-Jahr-Feier Univ. Innsbruck*, Innsbruck, 9–103.
- Bechstädt, T., Brandner, R., Mostler, H. and Schmidt, K.** (1978) Aborted rifting in the Triassic of the Eastern and Southern Alps. *N. Jb. Geol. Paläont. Abh.*, **156**, 157–178.
- Bernet, M., Zattin, M., Garver, J.I., Brandon, M.T. and Vance, J.A.** (2001) Steady-state exhumation of the European Alps. *Geology*, **29**, 35–38.
- Bertotti, G., ter Voorde, M., Cloething, S. and Picotti, V.** (1997) Thermomechanical evolution of the South Alpine rifted margin (North Italy): Constraints on the strength of passive continental margins. *Earth Planet. Sci. Lett.*, **146**, 181–193.
- Bertotti, G., Seward, D., Wijbrans, J., ter Voorde, M. and Hurford, A.J.** (1999) Crustal thermal regime prior to, during, and after rifting: A geochronological and modelling study of the Mesozoic South Alpine rifted margin. *Tectonics*, **18/2**, 185–200.
- Bertotti, G., Mosca, P., Juez, J., Polino, R. and Dunai, T.** (2006) Oligocene to Present kilometres scale subsidence and exhumation of the Ligurian Alps and the Tertiary Piedmont Basin (NW Italy) revealed by apatite (U–Th)/He thermochronology: Correlation with regional tectonics. *Terra Nova*, **18**, 18–25.
- Bielefeld, D.** (1998) *Reifebestimmungen an Kohlen des Grödner Sandsteins in Südtirol (Norditalien)*. Master’s thesis, Geol. Inst. Univ. Cologne, Germany, 87 pp.
- Blendinger, W.** (1985) Middle Triassic strike-slip tectonics and igneous activity of the Dolomites (Southern Alps). *Tectonophysics*, **113**, 105–121.
- Blendinger, W.** (1994) The carbonate factory of Middle Triassic buildups in the Dolomites, Italy: A quantitative analysis. *Sedimentology*, **41**, 1147–1159.
- Blendinger, W., Brack, P., Norborg, A.K. and Wulff-Pedersen, E.** (2004) Three-dimensional modelling of an isolated carbonate buildup (Triassic, Dolomites, Italy). *Sedimentology*, **51**, 297–314.
- Boni, M., Iannace, A., Torre, M. and Zamparelli V.** (1994) The Ladinian-Carnian reef facies of Monte Caramolo (Calabria Southern Italy). *Facies*, **30**, 101–118.
- Boomer, I., Whatley, R., Bassi, D., Fugagnoli, A. and Loriga, C.** (2001) An Early Jurassic oligohaline ostracod assemblage within the marine carbonate platform sequence of the Venetian Prealps, NE Italy. *Palaeogeogr. Palaeoclimatol. Palaeoecol.*, **166**, 331–344.
- Bosellini, A.** (1984) Progradation geometries of carbonate platforms: Examples from the Triassic of the Dolomites, Northern Italy. *Sedimentology*, **31**, 1–24.
- Bosellini, A.** (1988) Outcrop models for seismic stratigraphy: Examples from the Triassic of the Dolomites. In: *Atlas of Seismic Stratigraphy*, Vol. 2 (Ed. A.W. Bally), *AAPG Stud. Geol.*, **27**, 194–203.
- Bosellini, A.** (1989) Dynamics of Tethyan carbonate platforms. In: *Controls on Carbonate Platform and Basin Development* (Eds P.D. Crevello, J.J. Wilson, J.F. Sarg and J.F. Read), *SEPM Spec. Publ.*, **44**, 3–13.
- Bosellini, A. and Broglio Loriga, C.** (1971) I “Calcarei Grigi” di Rotzo (Giurassico Inferiore, Altopiano d’Asiago) e loro inquadramento nella paleogeografia e nella evoluzione tettono-sedimentaria delle Prealpi Venete). *Ann. Univ. Ferrara, N.S., Sez. IX Sci. Geol. Paleontol.*, **V/1**, 1–61.
- Bosellini, A. and Hardie, L.A.** (1985) Facies e cicli della Dolomia Principale delle Alpi Venete. *Mem. Soc. Geol. Ital.*, **30**, 245–266.
- Bosellini, A. and Stefani, M.** (1991) *The Rosengarten: A Platform-to-Basin Carbonate Section (Middle Triassic, Dolomites, Italy)*. Dolomieu Conference on Carbonate Platforms and Dolomitization, Guidebook Excursion C, 24 pp.
- Bosellini, A., Neri, C. and Stefani, M.** (1996) *Geometrie deposizionali e stratigrafia fisica a grande scala di piattaforme carbonatiche triassiche*. 78a riunione estiva, Soc. Geol. Ital., San Cassiano Guidebook, 36 pp.
- Bosence, D.W.J., Pomar, L., Waltham, D.A. and Lankester, T.H.G.** (1994) Computer modelling a Miocene carbonate platform, Mallorca, Spain. *AAPG Bull.*, **78**, 247–266.
- Bosscher, H. and Schlager, W.** (1993) Accumulation rates of carbonate platforms. *J. Geol.*, **101/3**, 345–355.
- Bowman, S.A. and Vail, P.R.** (1999) Interpreting the stratigraphy of the Baltimore Canyon section, offshore New Jersey with Phil, a stratigraphic simulator. In: *Numerical Experiments in Stratigraphy: Recent Advances in Stratigraphic and Sedimentologic Computer Simulations* (Eds J.W. Harbaugh, W.L. Watney, E.C. Rankey, R. Slingerland, R.H. Goldstein and E.K. Franseen), *SEPM Spec. Publ.*, **62**, 117–138.
- Brack, P. and Rieber, H.** (1993) Towards a better definition of the Anisian/Ladinian boundary: New biostratigraphical data and correlations of boundary sections from the Southern Alps. *Eclogae Geol. Helv.*, **86**, 415–527.
- Brack, P. and Rieber, H.** (1994) The Anisian/Ladinian boundary: Retrospective and new constraints. *Alberitiana*, **13**, 25–36.

- Brack, P., Mundil, R., Oberli, F., Meier, M. and Rieber, H.** (1996) Biostratigraphic and radiometric age data question the Milankovitch characteristics of the Latemar cycles (Southern Alps, Italy). *Geology*, **24**, 371–375.
- Brack, P., Mundil, R., Oberli, F., Meier, M. and Rieber, H.** (1997) Biostratigraphic and radiometric age data question the Milankovitch characteristics of the Latemar cycles (Southern Alps, Italy). Reply. *Geology*, **25**, 471–472.
- Brandner, R.** (1991) Geological setting and stratigraphy of the Schlern–Rosengarten buildup and Seiser Alm basin. In: *The Northern Margin of the Schlern/Sciliar Rosengarten/Catinaccio Platform* (Eds R. Brandner, E. Flügel, R. Koch and L.A. Yose), Dolomieu Conference on Carbonate Platforms and Dolomitization, Guidebook Excursion A, pp. 4–16.
- Broglio Loriga, C., Masetti, D. and Neri, C.** (1983) La formazione di Werfen (Scitico) delle Dolomiti occidentali: Sedimentologia e biostratigrafia. *Riv. Ital. Paleontol. Stratigr.*, **88**, 501–598.
- Buggisch, W.** (1978) Die Grödener Schichten (Perm, Südalpen). Sedimentologische und geochemische Untersuchungen zur Unterscheidung mariner und kontinentaler Sedimente. *Geol. Rundsch.*, **67**, 149–180.
- Buggisch, W. and Noé, S.** (1986) Upper Permian and Permian-Triassic Boundary of the Carnia (Bellerophon Formation, Tesero Horizon, Northern Italy). *Mem. Soc. Geol. Ital.*, **34**, 91–106.
- Büker, C.** (1996) *Absenkungs-, Erosions und Wärme-flussgeschichte des Ruhr-Beckens und des nordöstlichen Rechtsrheinischen Schiefergebirges*. Ber. Forsch. Jülich, **Jül-3319**, 212 pp.
- Carrapa, B., Wijbrans, J. and Bertotti, G.** (2003) Episodic exhumation in the Western Alps. *Geology*, **31**, 601–604.
- Claps, M., Masetti, D., Pedrielli, F. and Lucchi Garavello, A.** (1991) Analisi spettrale e cicli di Milankovitch in successioni cretatiche del sudalpino orientale. *Riv. Ital. Pal. Stratigr.*, **97**, 153–174.
- Cros, P.** (1966) Age Oligocène Supérieur d'un poudingue (du Monte Parei) dans les Dolomites centrales italiennes. *CR Somm. Soc. Géol. Fr.*, **7**, 250–252.
- D'Amico, C. and Del Moro, A.** (1988) Permian and Triassic Rb-Sr dating in the Permian rhyodacitic ignimbrites of Trentino (Southern Alps). *Rend. Soc. Ital. Mineral. Petrol.*, **43**, 171–180.
- De Zanche, V., Gianolla, P., Manfrin, S., Mietto, P. and Roghi, G.** (1995) A Middle Triassic back-stepping carbonate platform in the Dolomites (Italy): Sequence stratigraphy and biostratigraphy. *Mem. Sci. Geol.*, **47**, 135–155.
- Della Porta, G., Kenter, J.A.M. and Bahamonde, J.R.** (2004) Depositional facies and stratal geometry of an Upper Carboniferous prograding and aggrading high-relief carbonate platform (Cantabrian Mountains, N Spain). *Sedimentology*, **51**, 267–295.
- Dercourt, J., Gaetani, M., Vrielynck, B., Barrier, E., Biju-Duval, B., Brunet, M.F., Cadet, J.P., Crasquin, S. and Sandulescu, M.** (2000) *Atlas Peri-Tethys, Palaeogeographical Maps*. CCGM/CGMW, Paris: 24 maps and explanatory notes: I–XX, 269 pp.
- Dickinson, W.R., Armin, R.A., Beckvar, T.C., Goodlin, S.U., Janicke, R.A., Mark, R.D., Norris, G., Radcliff, G. and Wortman, A.A.** (1987) Geohistory analysis of rates of sediment accumulation and subsidence for selected California Basins. In: *Cenozoic Basin Development of Coastal California* (Eds V.R. Ingersoll and W.G. Ernst), pp. 1–23. Rubey Volume VI, Prentice-Hall, Englewood Cliffs, NJ.
- Dogliani, C.** (1983) Duomo Medio-Triassico nelle Dolomiti. *Rend. Soc. Geol. Ital.*, **6**, 13–16.
- Dogliani, C.** (1984) Triassic diapiric structures in the Central Dolomites. *Eclogae Geol. Helv.*, **77**, 261–285.
- Dogliani, C.** (1987) Tectonics of the Dolomites. *J. Struct. Geol.*, **9**, 181–193.
- Dogliani, C. and Bosellini, A.** (1987) Eoalpine and mesoalpine tectonics in the Southern Alps. *Geol. Rundsch.*, **76**, 735–754.
- Dogliani, C. and Goldhammer, R.K.** (1988) Compaction-induced subsidence in the margin of a carbonate platform. *Basin Res.*, **1**, 237–246.
- Dunkl, I., di Giulio, A. and Kuhlemann, J.** (2001) Combination of single-grain fission-track chronology and morphological analysis of detrital zircon crystals in provenance studies sources of the Macigno Formation (Apennines, Italy). *J. Sed. Res.*, **71**, 516–525.
- Egenhoff, S.O., Peterhänsel, A., Bechstadt, T., Zühlke, R. and Grötsch, J.** (1999) Facies architecture of an isolated carbonate platform: Tracing the cycles of the Latemar (Middle Triassic, Northern Italy). *Sedimentology*, **46**, 893–912.
- Emmerich, A., Glasmacher, U.A., Bauer, F., Bechstadt, T. and Zühlke, R.** (2005a) Meso-/Cenozoic basin and carbonate platform development in the SW-Dolomites unraveled by basin modelling and apatite FT analysis: Rosengarten and Latemar (Northern Italy). *Sed. Geol.*, **175**, 415–438.
- Emmerich, A., Zamparelli, V., Bechstadt, T. and Zühlke, R.** (2005b) The reefal margin and slope of a Middle Triassic carbonate platform: The Latemar (Dolomites, Italy). *Facies*, **50**, 573–614.
- Enos, P.** (1991) Sedimentary parameters for computer modelling. In: *Sedimentary Modelling: Computer Simulations and Methods for Improved Parameter Definition* (Eds E.K. Franseen, W.L. Watney, C.G.St.C. Kendall and W. Ross), *Kansas Geol. Surv. Bull.*, **233**, 63–99.
- Fitzgerald, P.G., Sorkhabi, R.B., Redfield T.F. and Stump, E.** (1995) Uplift and denudation of the central Alaska Range: A case study in the use of apatite fission track thermochronology to determine absolute uplift parameters. *J. Geophys. Res.*, **100**, 20175–20191.
- Flügel, E.** (2002) Triassic reef patterns. In: *Phanerozoic Reef Patterns* (Eds W. Kiessling, E. Flügel and J. Golonka), *SEPM Spec. Publ.*, **72**, 391–463.
- Fois, E. and Gaetani, M.** (1984) The recovery of reef-building communities and the role of Cnidarians in carbonate sequences of the Middle Triassic (Anisian) in the Italian Dolomites. *Palaeontogr. Am.*, **54**, 191–200.
- Gaetani, M., Fois, E., Jadoul, F. and Nicora, A.** (1981) Nature and evolution of the Middle Triassic carbonate buildups in the Dolomites (Italy). *Mar. Geol.*, **44**, 25–57.
- Gianolla, P. and Jacquini, T.** (1998) Triassic sequence stratigraphic framework of western European basins. In: *Mesozoic and Cenozoic Sequence Stratigraphy of European Basins* (Eds P.-C. de Graciansky, J. Hardenbol, T. Jacquini and P.R. Vail), *SEPM Spec. Publ.*, **60**, 643–650.

- Goldhammer, R.K. and Harris, M.T.** (1989) Eustatic controls on the stratigraphy and geometry of the Latemar buildup (Middle Triassic), the Dolomites of Northern Italy. In: *Controls on Carbonate Platform and Basin Development* (Eds P.D. Crevello, J.J. Wilson, J.F. Sarg and J.F. Read), *SEPM Spec. Publ.*, **44**, 323–338.
- Gradstein, F.M., Ogg, J.G., Smith, A.G. et al.** (Eds) (2004) *A Geologic Time Scale 2004*. Cambridge University Press, Cambridge, 589 pp.
- Greber, E., Leu, W., Bernoulli, D., Schuhmacher, M. and Wyss, R.** (1997) Hydrocarbon provinces in the Swiss Southern Alps – a gas geochemistry and basin modelling study. *Mar. Petrol. Geol.*, **14**, 3–25.
- Hardenbol, J., Thierry, J., Farley, M. B., Jacquin, T., de Graciansky, P.-C. and Vail, P. R.** (1998) Mesozoic and Cenozoic sequence chronostratigraphic framework of European basins. In: *Mesozoic and Cenozoic sequence stratigraphy of European Basins* (Eds P.-C. de Graciansky, J. Hardenbol, T. Jacquin and P.R. Vail), *SEPM Spec. Publ.*, **60**, 3–15.
- Hardie, L.A. and Hinnov, L.** (1997) Biostratigraphic and radiometric age data question the Milankovitch characteristics of the Latemar cycles (Southern Alps, Italy). *Comment. Geology*, **25**, 470–471.
- Harris, M.T.** (1994) The foreslope and toe-of-slope facies of the Middle Triassic Latemar buildup (Dolomites, Northern Italy). *J. Sed. Res.*, **B64**, 132–145.
- Hertle, M. and Littke, R.** (2000) Coalification pattern and thermal modelling of the Permo-Carboniferous Saar basin (SW-Germany). *Int. J. Coal Geol.*, **42**, 273–296.
- Hinnov, L. and Goldhammer, R.K.** (1991) Spectral analysis of the Middle Triassic Latemar limestone. *J. Sediment. Petrol.*, **61**, 1173–1193.
- Hsü, K.J.** (1971) Origin of the Alps and the western Mediterranean. *Nature*, **233**, 44–48.
- Hsü, K.J.** (1989) Time and place in Alpine orogenesis – the Fermor Lecture. In: *Alpine Tectonics* (Eds M.P. Coward, D. Dietrich and R.G. Park), *Geol. Soc. London Spec. Publ.*, **45**, 421–443.
- Hummel, K.** (1928) Das Problem des Fazieswechsels in der Mitteltrias der Südtiroler Dolomiten. *Geol. Rundsch.*, **19**, 223–228.
- Hummel, K.** (1932) Zur Stratigraphie und Faziesentwicklung der südalpinen Mitteltrias. *N. Jb. Mineral. Geol. Paläontol. Suppl.*, **68 B**, 403–462.
- Hunt, D. and Fitchen, W.M.** (1999) Compaction and the dynamics of carbonate-platform development: Insights from the Permian Delaware and Midlands Basins, Southeast New Mexico and West Texas, U.S.A. In: *Advances in Carbonate Sequence Stratigraphy: Application to Reservoirs, Outcrops and Models* (Eds P.M. Harris, A.H. Saller and J.A. Simo), *SEPM Spec. Publ.*, **63**, 75–106.
- Keim, L. and Schlager, W.** (2001) Quantitative compositional analysis of a Triassic carbonate platform (Southern Alps, Italy). *Sediment. Geol.*, **139**, 261–283.
- Kenter, J.A.M., Harris, P.M.M. and Porta, G.D.** (2005) Steep microbial boundstone-dominated platform margins – examples and implications. *Sediment. Geol.*, **178**, 5–30.
- Kenter, J.A.M., van Hoeflaken, F., Bahamonde, J.R., Bracco Gartner, Guido L., Keim, L. and Besems, R.E.** (2002) Anatomy and lithofacies of an intact and seismic-scale Carboniferous carbonate platform (Asturias, NW Spain): Analogues of hydrocarbon reservoirs in the Pricaspian Basin (Kazakhstan). In: *Paleozoic Carbonates of the Commonwealth of Independent States (CIS): Subsurface Reservoirs and Outcrop Analogues* (Eds W.G. Zempolich and H.E. Cook), *SEPM Spec. Publ.*, **74**, 181–203.
- Ketcham, R.A., Donelick, R.A. and Donelick, M.B.** (2000) AFTSolve: A program for multikinetic modelling of apatite fission-track data. *Geol. Mater. Res.*, **2(1)**, (electronic: 18 pages, 2 tables, 12 figures). Mineral. Soc. Am., Washington, DC.
- Kuhlemann, J., Dunkl, I., Brügel, A., Spiegel, C. and Frisch, W.** (2006) From source terrains of the Eastern Alps to the Molasse Basin: Detrital record of non-steady-state exhumation. *Tectonophysics*, **413**, 301–316.
- Laslett, G.M., Green, P.F., Duddy, I.R. and Gleadow, A.J.W.** (1987) Thermal annealing of fission tracks in apatite. 2. A quantitative analysis. *Chem. Geol.*, **65**, 1–13.
- Laubscher, H. and Bernoulli, D.** (1982) History and deformation of the Alps. In: *Mountain Building Processes* (Ed. K.J. Hsü), pp. 169–180. Academic Press, London.
- Lehrmann, D., Enos, P., Montgomery, P., Payne, J., Orchar, M., Bowring, S., Ramezani, J., Martin, M., Jiayong, W., HongMei, W., YouYi, Y., Jiafei, X. and Rongxi, L.** (2002) Integrated biostratigraphy, magnetostratigraphy and geochronology of the Olenikian-Anisian boundary in marine strata of Guandao section, Nanpanjiang Basin, South China: Implications for timing of biotic recovery from the end-Permian extinction. In: *I.U.G.S. Subcommission on Triassic Stratigraphy* (Ed. O. Piro), STS/IGCP 467 Field Meeting, Veszprém, Hungary, pp. 7–8.
- Leischner, K.** (1994) *Kalibration simulierter Temperaturgeschichten von Sedimentgesteinen*. Ber. Forsch. Jülich, **Jül-2909**, 309 pp.
- Leonardi, P.** (1962) Il gruppo dello Sciliar e le scogliere coralligene dolomitiche. *Ann. Univ. Ferrara, N.S., sez. IX*, **3**, 1–83.
- Leonardi, P.** (1967) *Le Dolomiti: Geologia dei Monti tra Isarco e Piave*. Manfrini, Rovereto, **1**, 1019 pp.
- Littke, R., Büker, C., Lückge, A., Sachsenhofer, R.F. and Welte, D.H.** (1994) A new evaluation of palaeo-heatflows and eroded thicknesses for the Carboniferous Ruhr basin, western Germany. *Int. J. Coal Geol.*, **26**, 155–183.
- Mair, V., Stingl, V., Krois, P. and Keim, L.** (1996) Die Bedeutung andesitischer und dazitischer Gerölle im Unterinntal-Tertiär (Tirol, Österreich) und im Tertiär des Mte. Parei (Dolomiten, Italien). *N. Jb. Geol. Paläontol. Abh.*, **199**, 369–394.
- Makhous, M. and Galushkin, Y.I.** (2004) *Basin Analysis and Modeling of the Burial, Thermal and Maturation Histories in Sedimentary Basins*. Éditions Technip, Paris, 400 pp.
- Martire, L.** (1996) Stratigraphy, facies and synsedimentary tectonics in the Jurassic Rosso Ammonitico Veronese (Altopiano di Asiago, NE Italy). *Facies*, **35**, 209–236.
- Masetti, M. and Neri, C.** (1980) L'Anisico della Val di Fassa (Dolomiti occidentali): Sedimentologia e paleogeografia. *Ann. Univ. Ferrara, N.S., sez. IX*, **7**, 1–19.

- Massari, F. and Neri, C.** (1997) The infill of a supradetachment(?) basin: The continental to shallow-marine Upper Permian succession in the Dolomites and Carnia (Italy). *Sediment. Geol.*, **110**, 181–221.
- Massari, F., Grandesso, P., Stefani, C. and Jobstraibizer, P.G.** (1986) A small polyhistory foreland basin evolving in a context of oblique convergence: The Venetian basin (Chattian to Recent, Southern Alps, Italy). In: *Foreland Basins* (Eds P.A. Allen and P. Homewood), *Int. Assoc. Sedimentol. Spec. Publ.*, **8**, 141–168.
- Massari, F., Conti, M.A., Fontana, D., Helmold, K., Mariotti, N., Neri, C., Nicosia, U., Ori, G.G., Pasini, M. and Pittau, P.** (1988) The Val Gardena sandstone and Bellerophon formation in the Bletterbach gorge (Alto Adige, Italy): Biostratigraphy and sedimentology. *Mem. Sci. Geol.*, **40**, 229–273.
- Massari, F., Neri, C., Pittau, P., Fontana, D. and Stefani, C.** (1994) Sedimentology, palynostratigraphy and sequence stratigraphy of a continental to shallow-marine rift-related succession: Upper Permian of the Eastern Southern Alps (Italy). *Mem. Sci. Geol.*, **46**, 119–243.
- Mastandrea, A., Neri, C. and Russo, F.** (1997) Conodont biostratigraphy of the S. Cassiano Formation surrounding the Sella Massif (Dolomites, Italy): Implications for sequence stratigraphic models of the Triassic of the Southern Alps. *Riv. Ital. Paleontol. Stratigr.*, **103**, 39–52.
- Maurer, F.** (1999) Wachstumsanalyse einer mitteltriadischen Karbonatplattform in den westlichen Dolomiten (Südalpen). *Eclogae Geol. Helv.*, **92**, 361–378.
- Maurer, F.** (2000) Growth mode of middle Triassic carbonate platforms in the Western Dolomites (Southern Alps, Italy). *Sediment. Geol.*, **134**, 275–286.
- Maurer, F. and Schlager, W.** (2003) Lateral variations in sediment composition and bedding in Middle Triassic interplatform basin (Buchenstein Formation, southern Alps, Italy). *Sedimentology*, **50**, 1–22.
- Maurer, F., Reijmer, J.J.G. and Schlager, W.** (2003) Quantification of input and compositional variations of calciturbidites in a Middle Triassic basinal succession (Seceda, Dolomites, Southern Alps). *Int. J. Earth Sci. (Geol. Rundsch.)*, **92**, 593–609.
- McKinney, M.L.** (1985) Mass extinction patterns of marine invertebrate groups and some implications for a causal phenomenon. *Paleobiology*, **11**, 227–233.
- Mojsisovics, E.** (1879) *Die Dolomitriffe von Südtirol und Venetien: Beiträge zur Bildungsgeschichte der Alpen*. Holder, Wien, 522 pp.
- Mundil, R., Brack, P., Meier, M., Rieber, H. and Oberli, F.** (1996) High resolution U/Pb dating of Middle Triassic volcanoclastics: Time-scale calibration and verification of tuning parameters for carbonate sedimentation. *Earth Planet. Sci. Lett.*, **141**, 137–151.
- Mundil, R., Metcalfe, I., Ludwig, K.R., Renne, P.R., Oberli, F. and Nicoll, R.S.** (2001) Timing of the Permian–Triassic biotic crisis: Implications from new zircon U/Pb age data (and their limitations). *Earth Planet. Sci. Lett.*, **187**, 131–145.
- Mundil, R., Zühlke, R., Bechstadt, T., Brack, P., Egenhoff, P., Meier, M., Oberli, F., Peterhänsel, A. and Rieber, H.** (2003) Cyclicities in Triassic platform carbonates: Synchronizing radio-isotopic and orbital clocks. *Terra Nova*, **15**, 81–87.
- Peters, K.E., Walters, C.C. and Mankiewicz, P.J.** (2006) Evaluation of kinetic uncertainty in numerical models of petroleum generation. *AAPG Bull.*, **90**, 387–403.
- Pia, J.** (1937) *Stratigraphie und Tektonik der Pragser Dolomiten in Südtirol*. Pia, Wien, 248 pp.
- Preto, N., Hinnov, L.A., Hardie, L.A. and De Zanche, V.** (2001) Middle Triassic orbital signature recorded in the shallow-marine Latemar carbonate buildup (Dolomites, Italy). *Geology*, **29**, 1123–1126.
- Preto, N., Spötl, C., Mietto, P., Gianaolla, P., Riva, A. and Manfrin, S.** (2005) Aragonite dissolution, sedimentation rates and carbon isotopes in deep-water hemipelagites (Livinallongo Formation, Middle Triassic, northern Italy). *Sed. Geol.*, **181**, 173–194.
- Raup, D.M.** (1979) Size of the Permo-Triassic bottleneck and its evolutionary implications. *Science*, **206**, 217–218.
- Reijmer, J.J.G.** (1998) Compositional variations during phases of progradation and retrogradation of a Triassic carbonate platform (Picco di Vallandro/Dürrenstein, Dolomites, Italy). *Geol. Rundsch.*, **87**, 436–448.
- Reijmer, J.J.G., ten Kate, W.G.H.Z., Sprenger, A. and Schlager, W.** (1991) Calciturbidite composition related to the exposure and flooding of a carbonate platform (Triassic, Eastern Alps). *Sedimentology*, **38**, 1059–1074.
- Rüffer, T. and Zühlke, R.** (1995) Sequence stratigraphy and sea-level changes in the Early to Middle Triassic of the Alps: A global comparison. In: *Sequence Stratigraphy and Depositional Response to Eustatic, Tectonic and Climatic Forcing* (Ed. B.U. Haq), pp. 161–207. Kluwer, Amsterdam.
- Sachsenhofer, R.F. and Littke, R.** (1993) Vergleich und Bewertung verschiedener Methoden zur Berechnung der Vitritreflexion am Beispiel von Bohrungen im Steirischen Tertiärbecken. *Zbl. Geol. Paläont.*, **1992/1**, 597–610.
- Sachsenhofer, R.F., Privalov, V.A., Zhykalyak, M.V., Büker, C., Panova, E.A., Rainer, T., Shymanovskyy, V.A. and Stephenson, R.** (2002) The Donets basin (Ukraine/Russia): Coalification and thermal history. *Int. J. Coal Geol.*, **49**, 33–55.
- Schlager, W.** (1981) The paradox of drowned reefs and carbonate platforms. *Geol. Soc. Am. Bull.*, **92**, 197–211.
- Schlager, W.** (1999) Scaling of sedimentation rates and drowning of reefs and carbonate platforms. *Geology*, **27**, 183–186.
- Schlager, W.** (2000) Sedimentation rates and growth potential of tropical, cool-water and mud-mound carbonate systems. In: *Carbonate Platform Systems: Components and Interactions* (Eds E. Insalaco, P.W. Skelton and T.J. Palmer), *Geol. Soc. Spec. Publ.*, **178**, 217–227.
- Schlager, W., Biddle, K.T. and Staffeu, J.** (1991) *Picco di Vallandro (Dürrenstein) a platform-basin transition in outcrop and seismic model*. Dolomieu Conference on Carbonate Platforms and Dolomitization, Guidebook Excursion **D**, 22 pp.
- Schulz, O. and Fuchs, H.W.** (1991) Kohle in Tirol: Eine historische kohlenpetrologische und lagerstättenkundliche Betrachtung. *Arch. Lagerst.forsch. Geol. B.-A.*, **13**, 123–213.
- Seeling, M., Emmerich, A., Bechstadt, T. and Zühlke, R.** (2005) Accommodation/sedimentation development and

- massive early marine cementation: Latemar vs. Concarana (Middle/Upper Triassic, Southern Alps). *Sed. Geol.*, **175**, 439–457.
- Senowbari-Daryan, B., Zühlke, R., Bechstädt, T. and Flügel, E.** (1993) Anisian (Middle Triassic) buildups of the Northern Dolomites (Italy): The recovery of reef communities after the Permian/Triassic crisis. *Facies*, **28**, 181–256.
- Smith, A.G.** (1971) Alpine deformation and the oceanic areas of the Tethys, Mediterranean and Atlantic. *Geol. Soc. Am. Bull.*, **82**, 2039–2070.
- Stach, E., Mackowsky, M., Teichmüller, M., Taylor, G.H., Chandra, D. and Teichmüller, R.** (1982) *Stach's Textbook of Coal Petrology*. Borntraeger, Berlin, 535 pp.
- Stock, H.W.** (1996) Planktonische Foraminiferen aus der Oberkreide der nordöstlichen Dolomiten (Italien). *Revue Paléobiol.*, **15**, 155–182.
- Sweeney, J.J. and Burnham, A.K.** (1990) Evaluation of a simple model of vitrinite reflectance based on chemical kinetics. *AAPG Bull.*, **74**, 1559–1570.
- Taylor, G.H., Teichmüller, M., Davis, A., Diessel, C.F.K., Littke, R. and Robert, P.** (1998) *Organic Petrology*. Borntraeger, Berlin, Stuttgart, 704 pp.
- Tippett, J.M. and Kamp, P.J.J.** (1995) Quantitative relationships between uplift and relief parameters for the Southern Alps, New Zealand, as determined by fission track analysis. *Earth Surf. Proc. Land.*, **20**, 153–175.
- Turcotte, D.L. and Schubert, G.** (1982) *Geodynamics – Applications of Continuum Physics to Geological Problems*. Wiley, New York, 450 pp.
- Turcotte, D.L. and Schubert, G.** (2002) *Geodynamics*. University Press, Cambridge, 456 pp.
- Trevisani, E.** (1991) Il Toarciano-Aaleniano nei settori centro-orientali della piattaforma di Trento (Prealpi Venete). *Riv. Ital. Paleontol. Stratigraf.*, **97**, 99–124.
- Trümpy, R.** (1982) Alpine palaeogeography: A reappraisal. In: *Mountain Building Processes* (Ed. K.J. Hsü), pp. 149–156. Academic Press, London.
- Twitchett, R.J.** (1999) Palaeoenvironments and faunal recovery after the end-Permian mass extinction. *Palaeogeogr. Palaeoclimatol. Palaeoecol.*, **154**, 27–37.
- Viel, G.** (1979a) Litostratigrafia Ladinica: Una revisione. Ricostruzione paleogeografica e paleostrutturale dell'area Dolomitico-Cadorina (Alpi Meridionali). I. Parte. *Riv. Ital. Paleontol. Stratigraf.*, **85**, 88–125.
- Viel, G.** (1979b) Litostratigrafia Ladinica: Una revisione. Ricostruzione paleogeografica e paleostrutturale dell'area Dolomitico-Cadorina (Alpi Meridionali). II. Parte. *Riv. Ital. Paleontol. Stratigraf.*, **85**, 297–352.
- Welte, D.H., Horsfield, B. and Baker, D.R.** (1997) *Petroleum and Basin Evolution*. Springer, Berlin, 535 pp.
- Winkler, W.** (1988) Mid- to Early Cretaceous flysch and melange formations in the western part of the Eastern Alps, palaeotectonic implications. *Jb. Geol. Bundesanst.*, **131**, 341–389.
- Winterer, E.L.** (1998) Palaeobathymetry of mediterranean Tethyan Jurassic pelagic sediments. *Mem. Soc. Geol. Ital.*, **53**, 97–131.
- Winterer, E.L. and Bosellini, A.** (1981) Subsidence and sedimentation on Jurassic passive continental margin, Southern Alps, Italy. *AAPG Bull.*, **65**, 394–421.
- Yugan, J., Wardlaw, B.R., Glenister, B.F. and Kotlyar, G.V.** (1997) Permian chronostratigraphic subdivisions. *Episodes*, **20**, 10–15.
- Zattin, M., Stefani, C. and Martin, S.** (2003) Detrital fission-track analysis and petrography as keys of Alpine exhumation: The examples of the Veneto foreland (Southern Alps, Italy). *J. Sediment. Res.*, **7**, 1051–1061.
- Zattin, M., Cuman, A., Fantoni, R., Martin, S., Scotti, P. and Stefani, C.** (2006) From Middle Jurassic heating to Neogene cooling: The thermochronological evolution of the southern Alps. *Tectonophysics*, **414**, 191–202.
- Zühlke, R.** (2000) Fazies, hochauflösende Sequenzstratigraphie und Beckenentwicklung im Anis (Mittlere Trias) der Dolomiten (Südalpin, Italien). *Gaea heidelberg.*, **6**, CD-ROM.
- Zühlke, R.** (2004) Integrated cyclostratigraphy of a model Mesozoic carbonate platform – the Latemar (Middle Triassic, Italy). In: *Cyclostratigraphy: Approaches and Case Histories* (Eds B. D'Argenio, A. Fisher, I. Premoli Silva, H. Weissert and V. Ferreri), *SEPM Spec. Publ.*, **81**, 183–211.
- Zühlke, R., Bechstädt, T. and Mundil, R.** (2003) Sub-Milankovitch and Milankovitch forcing on a model Mesozoic carbonate platform – the Latemar (Middle Triassic, Italy). *Terra Nova*, **15**, 69–80.